

# STABLE DERIVATIVE FREE GAUSSIAN MIXTURE VARIATIONAL INFERENCE FOR BAYESIAN INVERSE PROBLEMS \*

BAOJUN CHE<sup>§†</sup>, YIFAN CHEN<sup>‡</sup>, ZHENGHAO HUAN<sup>§</sup>, DANIEL ZHENGYU HUANG<sup>¶</sup>,  
AND WEIJIE WANG<sup>§</sup>

**Abstract.** This paper is concerned with the approximation of probability distributions known up to normalization constants, with a focus on Bayesian inference for large-scale inverse problems in scientific computing. In this context, key challenges include costly repeated evaluations of forward models, multimodality, and inaccessible gradients for the forward model. To address them, we develop a variational inference framework that combines Fisher-Rao natural gradient with specialized quadrature rules to enable derivative free updates of Gaussian mixture variational families. The resulting method, termed Derivative Free Gaussian Mixture Variational Inference (DF-GMVI), guarantees covariance positivity and affine invariance, offering a stable and efficient framework for approximating complex posterior distributions. The effectiveness of DF-GMVI is demonstrated through numerical experiments on challenging scenarios, including distributions with multiple modes, infinitely many modes, and curved modes in spaces with up to hundreds of dimensions. The method’s practicality is further demonstrated in a large-scale application, where it successfully recovers the initial conditions of the Navier-Stokes equations from solution data at positive times.

**Key words.** Bayesian Inverse Problems, Variational Inference, Derivative Free Methods, Multimodal, Gaussian Mixtures.

**AMS subject classifications.** 68Q25, 68R10, 68U05

**1. Introduction.** Sampling a target probability distribution known up to normalization constants is a classical problem in scientific computing. Specifically, in Bayesian inverse problems [39, 57], the goal is to recover an unknown parameter  $\theta \in \mathbb{R}^{N_\theta}$  from noisy observation  $y \in \mathbb{R}^{N_y}$ , through the equation

$$(1.1) \quad y = \mathcal{G}(\theta) + \eta.$$

Here,  $\mathcal{G}$  represents a forward map which, for the problems we consider, is nonlinear and requires solving a partial differential equation (PDE) for each evaluation. The observational noise  $\eta$  follows a Gaussian distribution:  $\eta \sim \mathcal{N}(0, \Sigma_\eta)$ . Within the Bayesian framework, we assign a Gaussian prior  $\mathcal{N}(r_0, \Sigma_0)$  to the unknown parameter  $\theta$ , resulting in a posterior distribution from which we aim to draw samples

$$(1.2) \quad \rho_{\text{post}}(\theta) \propto \exp(-\Phi_R(\theta)), \quad \Phi_R(\theta) = \frac{1}{2} \|\Sigma_\eta^{-\frac{1}{2}}(y - \mathcal{G}(\theta))\|^2 + \frac{1}{2} \|\Sigma_0^{-\frac{1}{2}}(\theta - r_0)\|^2.$$

It is worth noting that in this context,  $\Phi_R$  adopt a nonlinear least-squares structure, with an augmented map  $\mathcal{F}(\theta)$  satisfying

$$(1.3) \quad \Phi_R(\theta) = \frac{1}{2} \mathcal{F}(\theta)^T \mathcal{F}(\theta), \quad \mathcal{F}(\theta) = \begin{bmatrix} \Sigma_\eta^{-\frac{1}{2}}(y - \mathcal{G}(\theta)) \\ \Sigma_0^{-\frac{1}{2}}(r_0 - \theta) \end{bmatrix}.$$

\*Submitted to the editors DATE. The authors are in alphabetical order.

**Funding:** This work was funded by National Natural Science Foundation of China through grant 12471403 and the Fundamental Research Funds for the Central Universities of China.

<sup>†</sup>School of Mathematical Sciences, Nankai University, Tianjin, China (2111063@mail.nankai.edu.cn).

<sup>‡</sup>Courant Institute, New York University, NY (yifan.chen@nyu.edu)

<sup>§</sup>School of Mathematical Sciences, Peking University, Beijing, China (math\_hzh@stu.pku.edu.cn, wwj66285509350@stu.pku.edu.cn).

<sup>¶</sup>Corresponding author. Beijing International Center for Mathematical Research, Center for Machine Learning Research, Peking University, Beijing, China (huangdz@bicmr.pku.edu.cn).

The primary goal of this paper is to develop an efficient approach for the approximate sampling of such  $\rho_{\text{post}}(\theta)$ .

**1.1. Challenges.** For many Bayesian inverse problems in scientific applications, computing gradients of  $\Phi_R$  might be infeasible, as it requires derivatives of large-scale PDE-based models  $\mathcal{G}$  that may be black-box (e.g., climate models [55, 54]), use non-differentiable numerical methods (e.g., embedded boundary methods [51, 31, 30, 9] and adaptive mesh refinement [3, 6]), or model discontinuous physics (e.g., in fracture [48] or cloud modeling [58, 44]). Derivative free methods are thus needed; see a review of methodologies in subsection 1.3.2. While there are a few Markov Chain Monte Carlo (MCMC) and Sequential Monte Carlo (SMC) approaches that do not require gradients, they often require numerous function evaluations, particularly in high dimensions, to achieve convergence or mitigate weight collapse. This makes them impractical given the high computational cost of evaluating  $\mathcal{G}$ . Furthermore, the multimodality of  $\rho_{\text{post}}(\theta)$  causes MCMC methods to struggle with mode transitions [23, 24]. We note that missing modes can lead to significant prediction errors in scientific applications [59].

Variational inference offers a promising alternative, with black-box variational inference (BBVI) [52] being a popular approach for achieving derivative free sampling. BBVI typically relies on stochastic approximations to estimate gradients which exist high variance. This often makes BBVI unreliable, requiring variance reduction techniques and extensive time step tuning. Even with these improvements, small time steps are necessary to maintain stability (see subsection 5.2). Kalman methodology is also used to develop derivative-free variational inference methods [14, 32]. While these approaches can be effective for posterior distributions close to Gaussian or Gaussian mixture with separated components, they often become unstable in the presence of non-Gaussian or strongly curved modes (see [14, Appendix E]).

In this work, we explore guidelines for designing stable derivative free Gaussian mixture variational inference methods. Building on these guidelines, we propose a novel approach that requires no hyperparameter tuning while achieving both high accuracy and computational efficiency.

**1.2. Contributions.** Specifically, our contributions are as follows:

1. We propose derivative free quadrature rules for approximating the expectations of  $\Phi_R$  and Gaussian mixtures, their gradients, and their Hessians with respect to any Gaussian density. These methods are exact for linear  $\mathcal{F}$  implying low variance, and capture as much curvature information of  $\mathcal{F}$  as possible. Moreover, the computational cost, in terms of evaluating the forward mapping  $\mathcal{F}(\theta)$ , scales linearly with the dimensionality of  $\theta$ .
2. Building on these quadrature rules, we develop a derivative free variational inference approach that combines Fisher-Rao natural gradient and Gaussian mixture approximations (DF-GMVI). The DF-GMVI method ensures *covariance positivity* and exhibits *affine invariant properties*, which together contribute to its superior stability even when we use large time steps. These guidelines can also be applied to improve the robustness of other Gaussian mixture variational inference methods.
3. We demonstrate that DF-GMVI effectively captures multiple or even infinite modes, as well as curved modes, in model problems involving up to hundreds of dimensions. Additionally, it performs well in PDE-based applications, such as reconstructing the Navier-Stokes initial condition from solution data at positive times.

**1.3. Literature Review.** The review of relevant literature concerns variational inference, and related derivative free sampling approaches.

**1.3.1. Variational Inference.** The main idea of variational inference is to approximate a target density  $\rho_{\text{post}}$  within a variational family of densities  $Q$  from the view of optimization, that is, to identify the member of this family that minimizes an energy function  $\mathcal{E}$ :

$$\rho = \arg \min_{\rho \in Q} \mathcal{E}(\rho, \rho_{\text{post}}),$$

where the minimizer coincides with  $\rho_{\text{post}}$ . The energy function is often chosen as the Kullback-Leibler divergence (2.1). Along the gradient flow of the energy function,  $\frac{d\rho}{dt} = -\nabla_M \mathcal{E}(\rho, \rho_{\text{post}})$ , with respect to the metric  $M$ , the density  $\rho$  gradually converges towards the target density. In practice, variational inference methods can be categorized into two categories: non-parametric and parametric approaches.

In non-parametric variational inference, the variational distribution is represented by an interacting particle system. The choice of metrics [13] determines the gradient flow, including the Wasserstein gradient flow [35, 12, 40], Fisher-Rao gradient flow [47, 17, 11, 63], Wasserstein-Fisher-Rao gradient flow [45], Kalman-Wasserstein gradient flow [22] and Stein gradient flow [42]. The interacting particle system evolves according to the gradient flow, gradually approximating the target distribution. The convergence rate and accuracy depend on the number of particles used to represent the distribution and the quality of their representation.

In parametric variational inference, the variational densities used to approximate the target density are parametrized. A common choice for the variational family is the Gaussian, which leads to Gaussian variational inference [50, 40, 5]. To account for the geometric structure of parameters, the gradient is preconditioned by the Fisher information matrix, resulting in the Fisher-Rao *natural gradient* [1, 50]. This approach leverages Fisher information matrix as a substitute for the Hessian, thereby outperforming standard gradient descent [46]. Gaussian approximations have also been explored for Stein gradient flows [43] and Wasserstein gradient flows [40, 16]. However, the Gaussian approximation has limited expressive power, prompting the use of more flexible variational families, such as Gaussian mixture. These include Gaussian mixture approximation of the natural gradient flow [41, 14] and Wasserstein gradient flow [40, 34]. The present work focuses on Gaussian mixture approximation of the natural gradient flow, with an emphasis on stable and efficient derivative free approximations.

**1.3.2. Derivative Free Sampling Approaches.** A large class of derivative free sampling approaches are Markov chain Monte Carlo (MCMC) methods [26, 25], where a derivative free proposal is used to move particles. The main challenges of these methods are the absence of stopping criteria and slow convergence, which worsen as the dimensionality of the problem increases. Several improvements have been proposed to address these issues, such as enhancing the proposal distribution by preserving affine invariance (e.g., the stretch move method [27]) and leveraging parallelization (e.g., with multiple chains [21, 7, 60]). This work also incorporates these two strategies.

Another class of methods is Sequential Monte Carlo (SMC)[18, 56, 4], where particles and their associated weights are updated together using importance sampling. However, resampling is necessary to address issues such as particle degeneracy, sample impoverishment, and instability[19], which arise due to the lack of gradient flow structures.

Finally, in variational inference, a major approach is black-box variational inference [52], which employs stochastic approximation via Monte Carlo methods to estimate gradients. However, the high variance of these gradient estimates often results in unstable updates and slow convergence. To address these challenges, strategies such as incorporating variance reduction techniques and adaptive learning rates to stabilize the gradient estimates have been proposed in [52, 62]. Alternatively, gradient-based variational inference methods, such as Kalman-Wasserstein gradient flow [22] and Fisher-Rao gradient flow [14], avoid direct gradient computation by leveraging Stein’s lemma:  $\mathbb{E}_{\mathcal{N}(\theta; m, C)}[\nabla_{\theta} \mathcal{F}(\theta)] = C^{-1} \text{Cov}_{\mathcal{N}(\theta; m, C)}[\mathcal{F}(\theta), \theta]$ . This approach enables gradient estimation through quadrature rules originated from Kalman filtering techniques, such as the ensemble Kalman filter [20], the unscented Kalman filter [37, 36, 33], and the cubature Kalman filter [2]. Notably, the latter two achieve exactness for linear  $\mathcal{F}$ , indicating low variance. Despite these advancements, these approaches still require small time steps to mitigate instability, especially when the posterior is high-dimensional, exhibits multimodality, or involves complex dependencies. This work focuses on advancing quadrature rules for estimating gradients and even Hessians, which are crucial for developing stable, derivative-free variational inference methods.

**1.4. Organization.** The remainder of the paper is organized as follows. In section 2, we provide an overview of natural gradient variational inference, including both Gaussian and Gaussian mixture variational families. Section 3 introduces our Derivative Free Gaussian Mixture Variational Inference (DF-GMVI), and the related theoretical insights are presented in section 4. Numerical experiments are described in section 5, which serve to empirically validate the theory and demonstrate the effectiveness of the proposed framework for Bayesian inference. Finally, concluding remarks are provided in section 6.

**2. Natural Gradient Variational Inference.** In this section, we first briefly review natural gradient variational inference from the perspective of gradient flow. Then we discuss both the Gaussian variational family and the Gaussian mixture variational family in Sections 2.1 and 2.2, respectively. Variational inference aims to approximate the posterior distribution (1.2) by minimizing the Kullback–Leibler (KL) divergence [61, 5]

$$(2.1) \quad \text{KL}[\rho_a \|\rho_{\text{post}}] = \int \rho_a \log\left(\frac{\rho_a}{\rho_{\text{post}}}\right) d\theta$$

over a variational family of densities  $\rho_a$ , parameterized by  $a \in \mathbb{R}^{N_a}$ . When employing gradient descent, taking the continuous time limit, the parameter  $a$  evolves according to the gradient flow:

$$(2.2) \quad \frac{da}{dt} = -\nabla_a \text{KL}[\rho_a \|\rho_{\text{post}}].$$

The steepest descent direction can be interpreted as

$$(2.3) \quad -\nabla_a \text{KL}[\rho_a \|\rho_{\text{post}}] = \arg \min_{\sigma} \frac{\langle \nabla_a \text{KL}[\rho_a \|\rho_{\text{post}}], \sigma \rangle}{\sqrt{\langle \sigma, \sigma \rangle}},$$

where the numerator denotes the descent quantity along  $\sigma$  and the denominator denotes the length of  $\sigma$  under the Euclidean inner-product  $\langle \cdot, \cdot \rangle$  in  $\mathbb{R}^{N_a}$ . When a more general metric, induced by the inner product  $\langle \cdot, \mathfrak{M}(a) \cdot \rangle$  with metric tensor  $\mathfrak{M}(a)$  is

used, the steepest descent direction becomes

$$(2.4) \quad -\mathfrak{M}(a)^{-1}\nabla_a\text{KL}[\rho_a\|\rho_{\text{post}}] = \arg\min_{\sigma} \frac{\langle \nabla_a\text{KL}[\rho_a\|\rho_{\text{post}}], \sigma \rangle}{\sqrt{\langle \sigma, \mathfrak{M}(a)\sigma \rangle}}.$$

This modification leads to a different gradient flow for updating  $a$  as

$$(2.5) \quad \frac{da}{dt} = -\mathfrak{M}(a)^{-1}\nabla_a\text{KL}[\rho_a\|\rho_{\text{post}}].$$

The present work focuses on the natural gradient [1], where the metric tensor is the Fisher information matrix [53]

$$\mathfrak{M}(a) = \text{FIM}(a) := \int \frac{\partial \log \rho_a(\theta)}{\partial a} \frac{\partial \log \rho_a(\theta)}{\partial a}^T \rho_a(\theta) d\theta.$$

The Fisher-information matrix is related to the Hessian matrix of the KL-divergence [46], because the Taylor expansion of the KL-divergence (2.1) between  $\rho_a$  and its neighbor  $\rho_{a+da}$ , gives

$$(2.6) \quad \text{KL}[\rho_{a+da}\|\rho_a] = \frac{1}{2}da^T\text{FIM}(a)da + o(\|da\|^2).$$

Here we used the fact that  $\text{KL}[\rho_a\|\rho_a] = 0$  and  $\nabla_a\text{KL}[\rho_a\|\rho_a] = 0$  (the gradient is with respect to the first  $\rho_a$ ). Preconditioning the gradient with the Fisher information matrix inherently incorporates geometric information. Consequently, akin to Newton's method, the Fisher information matrix finds extensive application as a preconditioner to accelerate the optimization process in variational inference. This gives rise to the concept of natural gradient or natural gradient variational inference [1, 41], which corresponds to the following gradient flow:

$$(2.7) \quad \frac{da}{dt} = -\text{FIM}(a)^{-1}\nabla_a\text{KL}[\rho_a\|\rho_{\text{post}}].$$

Therefore, once the variational family is specified, discretizing the gradient flow introduced above enables the derivation of various practical sampling methods. In what follows, we provide two concrete examples.

**2.1. Gaussian Approximation.** Gaussian variational inference operates within a Gaussian parametric space, where the variational family

$$\rho_a^G(\theta) = \mathcal{N}(\theta; m, C)$$

represents a Gaussian parameterized by its mean  $m \in \mathbb{R}^{N_\theta}$  and covariance  $C \in \mathbb{R}^{N_\theta \times N_\theta}$ , collectively denoted by the parameter vector  $a := [m, C]$ . The Fisher information matrix of Gaussian is

$$(2.8) \quad \text{FIM}(a) = \begin{bmatrix} C^{-1} \\ X \end{bmatrix},$$

where  $X$  is a 4-th order tensor. Its action on any matrix  $Y \in \mathbb{R}^{N_\theta \times N_\theta}$  is given by

$$(2.9) \quad XY = \frac{1}{4}C^{-1}(Y + Y^T)C^{-1}.$$

Incorporating the Fisher information matrix into (2.7) and applying (1.2) yield the following natural gradient flow

$$(2.10) \quad \dot{m}_t = -C_t \mathbb{E}_{\rho_{a_t}}[\nabla \Phi_R], \quad \dot{C}_t = C_t - C_t \mathbb{E}_{\rho_{a_t}}[\nabla^2 \Phi_R] C_t.$$

By using the fact  $\dot{C}_t^{-1} = -C_t^{-1} \frac{dC_t}{dt} C_t^{-1}$ , we can rewrite the covariance evolution equation as

$$(2.11) \quad \dot{C}_t^{-1} = \mathbb{E}_{\rho_{a_t}}[\nabla^2 \Phi_R] - C_t^{-1}.$$

The above dynamics (2.10) is affine invariant [13, Section 5.4.1]. Consequently, when the posterior is Gaussian, it converges exponentially fast to the posterior at a rate of  $\mathcal{O}(e^{-t})$  [13, Theorem 5.6][22, 10, 8], where the exponent of the convergence rate is independent of the posterior. Furthermore, the time discretization of the natural gradient flow (2.10) exhibits superior stability. This stability arises from the fact that when the posterior density is log-concave, i.e., when  $\nabla^2 \Phi_R$  is positive semidefinite, the forward Euler discretization of (2.11) with  $0 < \Delta t < 1$  ensures covariance positivity:

$$C_{t+\Delta t}^{-1} = C_t^{-1} + \Delta t (\mathbb{E}_{\rho_{a_t}}[\nabla^2 \Phi_R] - C_t^{-1}) = (1 - \Delta t) C_t^{-1} + \Delta t \mathbb{E}_{\rho_{a_t}}[\nabla^2 \Phi_R] \succ 0,$$

provided that the approximation of  $\mathbb{E}_{\rho_{a_t}}[\nabla^2 \Phi_R]$  remains positive semidefinite.

**2.2. Gaussian Mixture Approximation.** Gaussian mixture variational inference considers the Gaussian mixture parametric space, where the variational family

$$\rho_a^{\text{GM}}(\theta) = \sum_{k=1}^K w_k \mathcal{N}(\theta; m_k, C_k)$$

is a  $K$ -component Gaussian mixture, parameterized by means  $m_k \in \mathbb{R}^{N_\theta}$ , covariances  $C_k \in \mathbb{R}^{N_\theta \times N_\theta}$  and weights  $w_k \in \mathbb{R}_{\geq 0}$ , collectively denoted by the parameter vector

$$a := [m_1, \dots, m_k, \dots, m_K, C_1, \dots, C_k, \dots, C_K, w_1, \dots, w_k, \dots, w_K].$$

Weights satisfy  $\sum_{k=1}^K w_k = 1$ . To compute the gradient flow in (2.7), we first evaluate the derivatives of the KL divergence in (2.1) with respect to  $a$ :

$$(2.12a) \quad \frac{\partial \text{KL}[\rho_a^{\text{GM}} \parallel \rho_{\text{post}}]}{\partial m_k} = w_k \int \mathcal{N}_k(\theta) \left( \nabla_\theta \log \rho_a^{\text{GM}} + \nabla_\theta \Phi_R \right) d\theta,$$

$$(2.12b) \quad \frac{\partial \text{KL}[\rho_a^{\text{GM}} \parallel \rho_{\text{post}}]}{\partial C_k} = \frac{w_k}{2} \int \mathcal{N}_k(\theta) \left( \nabla_\theta \nabla_\theta \log \rho_a^{\text{GM}} + \nabla_\theta \nabla_\theta \Phi_R \right) d\theta,$$

$$(2.12c) \quad \frac{\partial \text{KL}[\rho_a^{\text{GM}} \parallel \rho_{\text{post}}]}{\partial w_k} = \int \mathcal{N}_k(\theta) \left( \log \frac{\rho_a^{\text{GM}}}{\rho_{\text{post}}} + 1 \right) d\theta.$$

Here, we simplify the notation by denoting  $\mathcal{N}_k(\theta)$  as  $\mathcal{N}(\theta; m_k, C_k)$ . The steepest descent direction is determined by the following constrained optimization problem:

$$(2.13) \quad \arg \min_{\sigma} \frac{\langle \nabla_a \text{KL}[\rho_a \parallel \rho_{\text{post}}], \sigma \rangle}{\sqrt{\langle \sigma, \text{FIM}(a) \sigma \rangle}} \quad \text{s.t.} \quad \sum_{k=1}^K \sigma_{\dot{w}_k} = 0,$$

where  $\{\sigma_{\dot{w}_k}\}$  represents the descent directions corresponding to the weights. The Karush–Kuhn–Tucker conditions of (2.13) lead to the following natural gradient flow:

$$(2.14) \quad \begin{bmatrix} \dot{m}_k \\ \dot{C}_k \\ \dot{w}_k \end{bmatrix} = -(\text{FIM}(a))^{-1} \begin{bmatrix} w_k \int \mathcal{N}_k(\theta) \left( \nabla_\theta \log \rho_a^{\text{GM}} + \nabla_\theta \Phi_R \right) d\theta \\ \frac{w_k}{2} \int \mathcal{N}_k(\theta) \left( \nabla_\theta \nabla_\theta \log \rho_a^{\text{GM}} + \nabla_\theta \nabla_\theta \Phi_R \right) d\theta \\ \int \mathcal{N}_k(\theta) \left( \log \rho_a^{\text{GM}} + \Phi_R \right) d\theta + \lambda \end{bmatrix}.$$

Here  $\lambda \in \mathbb{R}$  is the Lagrangian multiplier, determined by the constraint  $\sum w_k = 1$ . Its value depends on  $\text{FIM}(a)$ .

The Fisher information matrix  $\text{FIM}(a)$  for Gaussian mixtures does not have a closed-form expression, and its inversion is computationally expensive. To improve efficiency, diagonal approximations of the Fisher information matrix have been used in the literature [14, Appendix C.8][41], leading to the following approximation:

$$(2.15) \quad \text{FIM}(a) \approx \text{Diag} \left( w_1 C_1^{-1}, \dots, w_K C_K^{-1}, w_1 X_1, \dots, w_K X_K, \frac{1}{w_1}, \dots, \frac{1}{w_K} \right).$$

Here each  $X_k$  is a 4-th order tensor, and its action on any matrix  $Y \in \mathbb{R}^{N_\theta \times N_\theta}$  is given by

$$(2.16) \quad X_k Y = \frac{1}{4} C_k^{-1} (Y + Y^T) C_k^{-1}.$$

Substituting the approximated Fisher information matrix (2.15) into the natural gradient flow (2.14) leads to the following equations:

$$(2.17) \quad \begin{aligned} \dot{m}_k &= -C_k \int \mathcal{N}_k(\theta) (\nabla_\theta \log \rho_a^{\text{GM}} + \nabla_\theta \Phi_R) d\theta, \\ \dot{C}_k &= -C_k \left( \int \mathcal{N}_k(\theta) (\nabla_\theta \nabla_\theta \log \rho_a^{\text{GM}} + \nabla_\theta \nabla_\theta \Phi_R) d\theta \right) C_k, \\ \dot{w}_k &= -w_k \int (\mathcal{N}_k(\theta) - \rho_a^{\text{GM}}) (\log \rho_a^{\text{GM}} + \Phi_R) d\theta. \end{aligned}$$

Here  $\lambda = -\int \rho_a^{\text{GM}} (\log \rho_a^{\text{GM}} + \Phi_R) d\theta$ . Similar to (2.11), the covariance evolution equation can be rewritten as:

$$(2.18) \quad \frac{dC_k^{-1}}{dt} = \int \mathcal{N}_k(\theta) (\nabla_\theta \nabla_\theta \log \rho_a^{\text{GM}} + \nabla_\theta \nabla_\theta \Phi_R) d\theta.$$

And the weight evolution equation can be reformulated as

$$(2.19) \quad \frac{d \log w_k}{dt} = - \int (\mathcal{N}_k(\theta) - \rho_a^{\text{GM}}) (\log \rho_a^{\text{GM}} + \Phi_R) d\theta$$

to ensure the weights remain positive. In the following, we also refer to (2.17) as the natural gradient flow, although involving an approximation of the Fisher information matrix. It is worth noting that when the mode number is  $K = 1$ , the natural gradient flow with Gaussian mixture approximation (2.17) reduces to the natural gradient flow with Gaussian approximation (2.10).

Designing effective schemes to discretize (2.17) remains challenging, particularly due to issues such as the computation of the Hessian matrix, the collapse of different modes, and the singularity of the covariance. A stable, derivative free approximation of (2.17) is the main focus of the present work.

**3. Derivative Free Gaussian Mixture Variational Inference.** In this section, we introduce a stable, derivative free approximation of (2.17) for Bayesian inverse problems, termed Derivative Free Gaussian Mixture Variational Inference (DF-GMVI). A key component of practical sampling algorithms is the design of effective quadrature rules. Commonly used methods include the mean-point approximation, unscented transformations [38, 36], cubature transformations [2], the Monte Carlo

approach, and stochastic approximation techniques [29]. The DF-GMVI method employs two quadrature rules, as defined in [Definitions 3.1](#) and [3.2](#), based the following considerations:

1. Numerical experiments presented in [Appendix A](#) demonstrate that, in this context, the mean-point approximation achieves superior convergence.
2. Building on the mean-point approximation, additional corrections are developed to approximate Hessian expectations, capturing as much curvature information of  $\mathcal{F}$  as possible, while maintaining linear complexity in the evaluation of  $\mathcal{F}$ . These corrections ensure *covariance positivity* and *affine invariance*, significantly improving the stability of the overall algorithm, as detailed in [section 4](#).

We begin by deriving a specialized quadrature rule to compute expectations of the following forms:

$$(3.1) \quad \mathbb{E}_{\mathcal{N}}[\Phi_R], \mathbb{E}_{\mathcal{N}}[\nabla_{\theta}\Phi_R], \text{ and } \mathbb{E}_{\mathcal{N}}[\nabla_{\theta}\nabla_{\theta}\Phi_R]$$

with respect to the Gaussian density  $\mathcal{N}(\theta; m, C)$  in a derivative free manner. Here, we assume access only to  $\mathcal{F}(\theta)$ , and recall that  $\Phi_R(\theta) = \frac{1}{2}\mathcal{F}(\theta)^T\mathcal{F}(\theta)$  has a nonlinear least-squares structure.

**DEFINITION 3.1.** *Given  $\theta \sim \mathcal{N}(\theta; m, C) \in \mathbb{R}^{N_{\theta}}$  and a hyperparameter  $\alpha > 0$ , we generate  $2N_{\theta} + 1$  quadrature points*

$$\theta_0 = m \quad \theta_i = m + \alpha[\sqrt{C}]_i \quad \theta_{N_{\theta}+i} = m - \alpha[\sqrt{C}]_i \quad (1 \leq i \leq N_{\theta}),$$

where  $\sqrt{C}$  is the square root matrix of  $C$ , such that  $C = \sqrt{C}\sqrt{C}^T$ . And  $[\sqrt{C}]_i$  denotes its  $i$ -th column. Given  $\mathcal{F} : \mathbb{R}^{N_{\theta}} \rightarrow \mathbb{R}^{N_x}$ , we compute vectors

$$(3.2) \quad c = \mathcal{F}(\theta_0), \quad b_i = \frac{\mathcal{F}(\theta_i) - \mathcal{F}(\theta_{N_{\theta}+i})}{2\alpha}, \quad a_i = \frac{\mathcal{F}(\theta_i) + \mathcal{F}(\theta_{N_{\theta}+i}) - 2\mathcal{F}(\theta_0)}{2\alpha^2} \quad (1 \leq i \leq N_{\theta}),$$

and denote  $B = [b_1; b_2; \dots; b_{N_{\theta}}] \in \mathbb{R}^{N_x \times N_{\theta}}$  and  $A = [a_1; a_2; \dots; a_{N_{\theta}}] \in \mathbb{R}^{N_x \times N_{\theta}}$ . The expectation of the function is then approximated as

$$(3.3) \quad \mathbb{E}_{\mathcal{N}}[\Phi_R] = \frac{1}{2}\mathbb{E}_{\mathcal{N}}[\mathcal{F}(\theta)^T\mathcal{F}(\theta)] \approx \frac{1}{2}c^T c.$$

The expectation of the gradient is approximated as

$$(3.4) \quad \mathbb{E}_{\mathcal{N}}[\nabla_{\theta}\Phi_R] = \frac{1}{2}\mathbb{E}_{\mathcal{N}}[\nabla_{\theta}(\mathcal{F}(\theta)^T\mathcal{F}(\theta))] \approx \sqrt{C}^{-T} B^T c.$$

The expectation of the Hessian is approximated as

$$(3.5) \quad \mathbb{E}_{\mathcal{N}}[\nabla_{\theta}\nabla_{\theta}\Phi_R] = \frac{1}{2}\mathbb{E}_{\mathcal{N}}[\nabla_{\theta}\nabla_{\theta}(\mathcal{F}(\theta)^T\mathcal{F}(\theta))] \approx \sqrt{C}^{-T} (6\text{Diag}(A^T A) + B^T B)\sqrt{C}^{-1},$$

where  $\text{Diag}(\cdot)$  extracts the diagonal elements of a matrix to form a diagonal matrix.

To reach [Definition 3.1](#), we first define  $\tilde{\mathcal{F}}(\tilde{\theta}) = \mathcal{F}(m + \sqrt{C}\tilde{\theta})$ . The expectations of  $\Phi_R(\theta)$  and its gradient in [\(3.3\)](#) and [\(3.4\)](#) are then approximated using the mean-point approximation with the finite difference approximation of the gradient



$\nabla_{\tilde{\theta}} \tilde{\mathcal{F}}(0)^T$ , as given in (3.2). The expectation of the Hessian in (3.5) can be interpreted as a correction that incorporates curvature information into the mean-point approximation in the Gaussian Newton formulation,  $\sqrt{C}^{-T} (B^T B) \sqrt{C}^{-1}$ . The derivation of the additional terms  $\sqrt{C}^{-T} (6\text{Diag}(A^T A)) \sqrt{C}^{-1}$  proceeds as follows: We assume that  $\tilde{\mathcal{F}}(\tilde{\theta}) = A\tilde{\theta} \odot \tilde{\theta} + B\tilde{\theta} + c$ , where  $\theta \odot \theta$  denoting elementwise product. The column vectors of matrices  $A$  and  $B$  are approximated by finite differences given in (3.2). Under this assumption, the expectation of the Hessian has an analytical form:

$$\begin{aligned} \frac{1}{2} \mathbb{E}_{\mathcal{N}} \left[ \nabla_{\theta} \nabla_{\theta} (\mathcal{F}(\theta)^T \mathcal{F}(\theta)) \right] &= \sqrt{C}^{-T} \mathbb{E}_{\tilde{\mathcal{N}}(0, I)} [\nabla_{\tilde{\theta}} \nabla_{\tilde{\theta}} \tilde{\mathcal{F}}(\tilde{\theta})^T \tilde{\mathcal{F}}(\tilde{\theta}) + \nabla_{\tilde{\theta}} \tilde{\mathcal{F}}(\tilde{\theta})^T \nabla_{\tilde{\theta}} \tilde{\mathcal{F}}(\tilde{\theta})] \sqrt{C}^{-1} \\ &= \sqrt{C}^{-T} (D + 2\text{Diag}(A^T c) + B^T B) \sqrt{C}^{-1}, \end{aligned} \quad \blacksquare$$

where  $D$  is a diagonal matrix with  $D_{jj} = 2 \sum_k a_j^T a_k + 4a_j^T a_j$ . To ensure covariance positivity, we retain only the positive definite part of this expectation, resulting in (3.5).

Moreover, it is worth noticing the quadrature rule approximation (3.5) achieves exactness when  $\mathcal{F}$  is linear. However, black-box variational inference [52] formulates this term as follows:

$$\mathbb{E}_{\mathcal{N}} [\nabla_{\theta} \nabla_{\theta} \Phi_R(\theta)] = 2 \int \nabla_C \mathcal{N}(\theta; m, C) \Phi_R(\theta) d\theta = C^{-1} \mathbb{E}_{\mathcal{N}} \left[ ((\theta - m)(\theta - m)^T - C) \Phi_R \right] C^{-1}, \quad \blacksquare$$

which is derived using integration by parts. Evaluating this requires computing the expectation of a highly nonlinear matrix function. Even when  $\mathcal{F}$  is linear, using either the unscented [38, 36] or cubature [2] transformations does not provide an accurate approximation. And stochastic approximation suffers from high variance, which slows convergence (see subsection 5.2).

Then, we develop the quadrature rule for approximating the expectation of  $\log \rho_a^{\text{GM}}$  and its derivatives used in (2.17). \blacksquare

**DEFINITION 3.2.** *Given Gaussian mixture  $\rho_a^{\text{GM}}(\theta) = \sum_{k=1}^K w_k \mathcal{N}(\theta; m_k, C_k)$ , the expectation of  $\log \rho_a^{\text{GM}}(\theta)$  and its gradient with respect to its Gaussian component  $\mathcal{N}_k(\theta) = \mathcal{N}(\theta; m_k, C_k)$  are approximated as*

$$(3.6) \quad \mathbb{E}_{\mathcal{N}_k} [\log \rho_a^{\text{GM}}(\theta)] \approx \log \rho_a^{\text{GM}}(m_k) \quad \mathbb{E}_{\mathcal{N}_k} [\nabla_{\theta} \log \rho_a^{\text{GM}}(\theta)] \approx \nabla_{\theta} \log \rho_a^{\text{GM}}(m_k).$$

*The expectation of the Hessian of  $\log \rho_a^{\text{GM}}(\theta)$  with respect to its Gaussian component  $\mathcal{N}_k$  is approximated as*

$$\begin{aligned} &\mathbb{E}_{\mathcal{N}_k} \left[ \nabla_{\theta} \nabla_{\theta} \log \rho_a^{\text{GM}}(\theta) \right] \\ &= -\mathbb{E}_{\mathcal{N}_k} \left[ \frac{\left( \sum_i w_i v_i \mathcal{N}_i(\theta) \right) \left( \sum_i w_i v_i \mathcal{N}_i(\theta) \right)^T}{\rho_a^{\text{GM}}(\theta)^2} + \frac{\sum_i w_i \left( C_i^{-1} - v_i v_i^T \right) \mathcal{N}_i(\theta)}{\rho_a^{\text{GM}}(\theta)} \right] \\ (3.7) \quad &= \mathbb{E}_{\mathcal{N}_k} \left[ \frac{\sum_{i < j} w_i w_j (v_i - v_j) (v_i - v_j)^T \mathcal{N}_i(\theta) \mathcal{N}_j(\theta)}{\rho_a^{\text{GM}}(\theta)^2} \right] - \mathbb{E}_{\mathcal{N}_k} \left[ \frac{\sum_i w_i \mathcal{N}_i(\theta) C_i^{-1}}{\rho_a^{\text{GM}}(\theta)} \right] \\ &\approx \frac{\sum_{i < j} w_i w_j (v_i(m_k) - v_j(m_k)) (v_i(m_k) - v_j(m_k))^T \mathcal{N}_i(m_k) \mathcal{N}_j(m_k)}{\rho_a^{\text{GM}}(m_k)^2} - C_k^{-1}. \end{aligned}$$

Here we denote  $v_i(\theta) = C_i^{-1}(\theta - m_i)$ .

The proposed quadrature rule in [Definition 3.2](#) is *consistent* with [Definition 3.1](#), which is important because the variational inference relies on the balance of these two terms. Specifically, the expectation of  $\log \rho_a^{\text{GM}}(\theta)$  and its gradient are computed using the mean-point approximation. For the Hessian approximation in [\(3.7\)](#), it is decomposed into two terms. The first term is approximated using the mean-point approximation. The second term is approximated as  $C_k^{-1}$ , which is a correction to the mean-point approximation. This correction satisfies the following equality:

$$\sum_k w_k \mathbb{E}_{\mathcal{N}_k} \left[ \frac{\sum_i w_i \mathcal{N}_i(\theta) C_i^{-1}}{\rho_a^{\text{GM}}(\theta)} \right] = \int \sum_i w_i \mathcal{N}_i(\theta) C_i^{-1} d\theta = \sum_k w_k C_k^{-1}.$$

When  $K = 1$ , this correction becomes exact. This correction ensures covariance positivity, significantly enhancing the stability of the algorithm (see [Proposition 4.1](#)).

Finally, we update the covariances, means, and weights sequentially using a forward Euler scheme from time  $t$  to time  $t + \Delta t$  with time step  $\Delta t$ . For the mean update, we use the updated covariance  $C_k(t + \Delta t)$  in a Gauss–Seidel manner on the right-hand side.

$$\begin{aligned} (3.8) \quad C_k^{-1}(t + \Delta t) &= C_k^{-1}(t) + \Delta t \text{QR}_{\mathcal{N}_k} \{ \nabla_\theta \nabla_\theta \log \rho_a^{\text{GM}}(t) + \nabla_\theta \nabla_\theta \Phi_R \}, \\ m_k(t + \Delta t) &= m_k(t) - \Delta t C_k(t + \Delta t) \text{QR}_{\mathcal{N}_k} \{ \nabla_\theta \log \rho_a^{\text{GM}}(t) + \nabla_\theta \Phi_R \}, \\ \log w_k(t + \Delta t) &= \log w_k(t) - \Delta t \text{QR}_{\mathcal{N}_k} \{ \log \rho_a^{\text{GM}}(t) + \Phi_R \}. \end{aligned}$$

Here, QR denotes the quadrature rules as defined in [Definitions 3.1](#) and [3.2](#), and  $\mathcal{N}_k$  denotes the  $k$ -th Gaussian component at time  $t$ . We then normalize  $w_k(t + \Delta t)_{k=1}^K$  and, for efficiency, set a lower bound of  $w_k$  at a default value of  $10^{-8}$  during normalization. The computational cost with respect to evaluating  $\mathcal{F}$  is  $(2N_\theta + 1)KN_t$ . This is because evaluating the quadrature rule in [Definition 3.1](#) requires computing  $\mathcal{F}$  at  $2N_\theta + 1$  quadrature points for each Gaussian mode, where  $N_t$  represents the total number of time steps. It is worth mentioning the evaluation of  $\mathcal{F}$  at the  $(2N_\theta + 1)K$  quadrature points can be performed in an embarrassingly parallel manner.

**4. Theoretical Insight.** In this section, we present the theoretical insights underlying the proposed DF-GMVI method, including its *covariance positivity-preserving* and *affine invariance* properties. These insights are also applied to design adaptive time-stepping schemes and select gradient flows, which significantly enhance the performance of other Gaussian mixture variational inference methods (see [subsection 5.2](#)).

A common issue with Gaussian mixture-based sampling methods is instability due to the covariance matrix becoming singular or non-positive. The following proposition establishes a condition on the time step  $\Delta t$  that ensures the covariance matrix remains positive definite during the update process, which relies on our design of the quadrature rules used for approximating Hessian expectations in [section 3](#). The proposition guarantees that we can choose a sufficiently large  $\Delta t$ , enabling faster convergence without introducing numerical instability (see [section 5](#)).

**PROPOSITION 4.1.** *For the DF-GMVI algorithm described in [\(3.8\)](#), if  $0 < \Delta t < 1$ , then  $C_k$  remains positive definite.*

*Proof.* Incorporating the quadrature rules from [\(3.5\)](#) and [\(3.7\)](#) into [\(3.8\)](#), the

update rule for  $C_k$  becomes

$$\begin{aligned}
(4.1) \quad C_k^{-1}(t + \Delta t) &= C_k^{-1}(t) + \Delta t \text{QR}_{\mathcal{N}_k} \{ \nabla_{\theta} \nabla_{\theta} \log \rho_a^{\text{GM}}(t) + \nabla_{\theta} \nabla_{\theta} \Phi_R \} \\
&= C_k^{-1}(t) + \Delta t \left( \sqrt{C}^{-T} (6\text{Diag}(A^T A) + B^T B) \sqrt{C}^{-1} - C_k^{-1} \right. \\
&\quad \left. + \frac{\sum_{i < j} w_i w_j (v_i(m_k) - v_j(m_k)) (v_i(m_k) - v_j(m_k))^T \mathcal{N}_i(m_k) \mathcal{N}_j(m_k)}{\rho_a^{\text{GM}}(m_k)^2} \right) \\
&= (1 - \Delta t) C_k^{-1}(t) + \Delta t \left( \sqrt{C}^{-T} (6\text{Diag}(A^T A) + B^T B) \sqrt{C}^{-1} \right. \\
&\quad \left. + \frac{\sum_{i < j} w_i w_j (v_i(m_k) - v_j(m_k)) (v_i(m_k) - v_j(m_k))^T \mathcal{N}_i(m_k) \mathcal{N}_j(m_k)}{\rho_a^{\text{GM}}(m_k)^2} \right). \blacksquare
\end{aligned}$$

Since the matrix within the brackets is always positive semidefinite and  $(1 - \Delta t)C_k^{-1}(t)$  is positive definite, we conclude that  $C_k^{-1}(t + \Delta t)$  is also positive definite.  $\square$

Moreover, sampling methods are said to be *affine invariant* if their behavior remains unchanged under any invertible affine transformation. This property makes these methods especially effective for highly anisotropic posterior distributions [27, 21]. Their effectiveness arises from consistent performance across coordinate systems related by affine transformations. Specifically, the convergence properties of these methods can be understood by examining the optimal coordinate system, which minimizes anisotropy to the fullest extent, across all affine transformations. The following proposition establishes a restricted affine invariance of DF-GMVI method.

**PROPOSITION 4.2.** *The sampling algorithm applied to the posterior distribution, which is proportional to  $e^{-\Phi_R(\theta)}$ , produces Gaussian mixture approximations parameterized by  $\{m_k(t), C_k(t), w_k(t)\}_{k=1}^K$ . When the algorithm is applied to the transformed posterior, with  $\tilde{\Phi}_R(\tilde{\theta}) = \Phi_R(T^{-1}(\tilde{\theta} - d))$ , under any invertible affine mapping  $\varphi: \theta \rightarrow \tilde{\theta} = T\theta + d$ , where  $T \in \mathcal{T}$  is an invertible matrix and  $d$  is a translation vector, it produces updated parameters  $\{\tilde{m}_k(t), \tilde{C}_k(t), \tilde{w}_k(t)\}_{k=1}^K$ . The algorithm is said to be  $\mathcal{T}$ -invariant if the following holds:*

$$\tilde{w}_k(t) = w_k(t), \quad \tilde{m}_k(t) = Tm_k(t) + d, \quad \tilde{C}_k(t) = TC_k(t)T^T.$$

Then, we have:

1. The natural gradient flow defined by (2.17) is affine invariant, i.e.,  $\mathcal{T}$  contains all invertible matrices.
2. The DF-GMVI algorithm (3.8) is  $\mathcal{T}$ -invariant, when using Cholesky decomposition to compute the square root matrix  $\sqrt{C}$  in Definition 3.1, where  $\mathcal{T}$  denotes the group of invertible lower triangular matrices.

We provide a proof of this proposition in Appendix B. The affine invariance is restricted because the Cholesky decomposition of the covariance is only invariant for lower triangular matrix group. The affine invariance enables the DF-GMVI method and variational inference methods based on natural gradient flow (2.17) to converge faster than other gradient flows with Gaussian mixture approximations, as further demonstrated numerically in subsection 5.2.

**5. Numerical Study.** In this section, we present numerical studies regarding the proposed DF-GMVI method. We focus on posterior distributions of unknown parameters or fields arising in inverse problems that may exhibit multiple modes. Three types of model problems are considered:

1. A one-dimensional bimodal problem from [14]: we use this problem as a proof-of-concept example. Our result shows that the convergence rate remains unchanged no matter how overlapped the two modes are. Additionally, DF-GMVI outperforms the derivative free Gaussian mixture Kalman inversion presented in [14].
2. Several multi-dimensional problems: we use these problems to demonstrate that DF-GMVI is robust with respect to the posterior featuring multiple modes, infinite many modes, and modes with narrow and curved shapes. And the convergence rate remains robust across different problem dimensionalities. Additionally, we compare DF-GMVI with other state-of-the-art sampling approaches, including Gaussian mixture variational inference methods leveraging gradient or Hessian information, BBVI, and MCMC methods, to highlight its strengths. Notably, the theoretical insights presented in [section 4](#) are general and are used to design adaptive time-stepping schemes that significantly enhance the robustness of these comparable Gaussian mixture variational inference methods.
3. Navier-Stokes problem: we consider the inverse problem of recovering the initial velocity field of a Navier-Stokes flow. The problem is structured to exhibit symmetry, resulting in two modes in the posterior distribution. We demonstrate that DF-GMVI effectively captures both modes, highlighting its potential for tackling multimodal problems in large-scale, high-dimensional applications.

For all tests, we use  $\Delta t = 0.5$  and run 200 iterations, resulting in a total time of  $T = 100$ . We set  $\alpha = 10^{-3}$  in the derivative free quadrature rule in [Definition 3.1](#). Our code is available online: <https://github.com/PKU-CMEGroup/InverseProblems.jl/tree/master/Derivative-Free-Variational-Inference>.

**5.1. One-Dimensional Problems.** In this subsection, we consider the 1D bimodal inverse problem from [14], associated with the forward model

$$y = \mathcal{G}(\theta) + \eta \quad \text{with} \quad y = 1, \quad \mathcal{G}(\theta) = \theta^2.$$

The prior is  $\rho_{\text{prior}} \sim \mathcal{N}(3, 2^2)$  and consider different noise levels:

$$\text{Case A: } \eta \sim \mathcal{N}(0, 0.2^2);$$

$$\text{Case B: } \eta \sim \mathcal{N}(0, 0.5^2);$$

$$\text{Case C: } \eta \sim \mathcal{N}(0, 1.0^2);$$

$$\text{Case D: } \eta \sim \mathcal{N}(0, 1.5^2).$$

Note that the overlap between these two modes increases as the noise level rises. In case A, the two modes are well separated, while in case D, they are nearly indistinguishable (See [Figure 1](#)).

We apply DF-GMVI with  $K = 2, 10, \text{ and } 40$  modes, each randomly initialized according to the prior distribution with equal weights. The converged density estimations at the 200th iteration are shown in [Figure 1](#), with each row corresponding to a case (A to D). The reference density is plotted in grey. For  $K = 10$  and 40, the estimated densities closely align with the reference. The fourth panel in each row displays the total variation error at each iteration, calculated as  $\int |\rho - \rho_{\text{ref}}| d\theta$ . Increasing  $K$  improves performance, unlike the Gaussian Mixture Kalman Inversion method proposed in [14], which suffers from mode collapse. Our approach outperforms that method while maintaining the same computational cost and derivative free property.

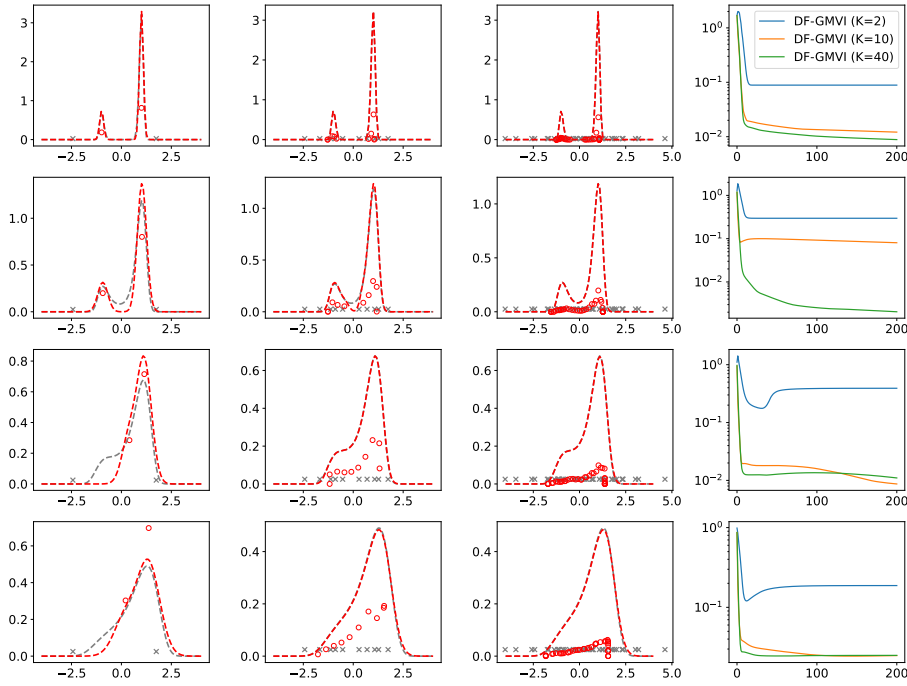


Fig. 1: The one-dimensional bimodal problem with  $\Sigma_\eta$  values of  $0.2^2$  (top),  $0.5^2$  (top middle),  $1.0^2$  (bottom middle), and  $1.5^2$  (bottom) is shown. Each panel displays the reference posterior distribution (gray dashed lines) alongside the posterior distributions estimated by DF-GMVI (red dashed lines) with mode numbers  $K = 2, 10, 40$  (from left to right). The mean  $m_k$  of each Gaussian component is marked by red circles, and the initial means are indicated by gray crosses, with their  $y$ -values corresponding to the respective weights (demonstrating no mode collapse). The fourth figure shows the total variation distance between the reference posterior distribution and the DF-GMVI estimated posteriors.

**5.2. Multi-Dimensional Problems.** In this subsection, we first examine several 2D sampling problems, along with their 100-dimensional modified versions. We then conclude with a comprehensive comparison to other state-of-the-art sampling approaches. For the 2D sampling problems, we define  $\Phi_R(\theta) = \frac{1}{2}\mathcal{F}(\theta)^T\mathcal{F}(\theta)$ , where  $\theta = [\theta_{(1)}, \theta_{(2)}]^T \in \mathbb{R}^2$ , and  $\mathcal{F}(\theta)$  is defined as follows.

Case A : The distribution is a Gaussian with

$$\mathcal{F}(\theta) = y - A\theta \quad A = \begin{bmatrix} 1 & 1 \\ 1 & 2 \end{bmatrix} \quad \text{and} \quad y = \begin{bmatrix} 0 \\ 1 \end{bmatrix}.$$

Case B : The distribution has four modes with different weights [14, Appendix D]

$$\mathcal{F}(\theta) = y - \begin{bmatrix} (\theta_{(1)} - \theta_{(2)})^2 \\ (\theta_{(1)} + \theta_{(2)})^2 \\ \theta_{(1)} \\ \theta_{(2)} \end{bmatrix} \quad \text{and} \quad y = \begin{bmatrix} 4.2297 \\ 4.2297 \\ 0.5 \\ 0.0 \end{bmatrix}.$$

Case C : The distribution is circular in shape [14, Appendix E], with its mass concentrated along an elliptical region,

$$\mathcal{F}(\theta) = 2(y - \theta^T A \theta) \quad \text{and} \quad A = \begin{bmatrix} 1 & 1 \\ 1 & 2 \end{bmatrix} \quad y = [1].$$

Case D : The distribution follows the Rosenbrock function, which has a characteristic “banana” shape [27], with

$$\mathcal{F}(\theta) = \frac{1}{\sqrt{10}} \left( y - \begin{bmatrix} 10(\theta_{(2)} - \theta_{(1)}^2) \\ \theta_{(1)} \end{bmatrix} \right) \quad \text{and} \quad y = \begin{bmatrix} 0 \\ 1 \end{bmatrix}.$$

Case E : The distribution is an extension of the Rosenbrock function [15] and is characterized by its bimodal, “banana” shaped density.

$$\mathcal{F}(\theta) = y - \begin{bmatrix} \log(100(\theta_{(2)} - \theta_{(1)}^2)^2 + (1 - \theta_{(1)})^2)/0.3 \\ \theta_{(1)} \\ \theta_{(2)} \end{bmatrix} \quad \text{and} \quad y = \begin{bmatrix} \log(101) \\ 0 \\ \blacksquare \\ 0 \end{bmatrix}.$$

We apply DF-GMVI with  $K = 10, 20$ , and  $40$  modes, each randomly initialized as  $\mathcal{N}(0, I)$  with equal weights. The density estimations at the 200th iteration are shown in Figure 2, with each row corresponding to a case (A to D). In each row, the reference density is displayed in the first panel, followed by the results from DF-GMVI with  $K = 10, 20$ , and  $40$  modes. The estimated densities closely match the reference. The fourth panel in each row shows the error in terms of total variation over the iterations. DF-GMVI effectively captures multiple modes (Cases B and E), densities characterized by narrow, curved valleys (Cases D and E), which typically pose challenges for sampling methods, as well as densities with infinitely many maximum a posteriori points (Case C). The fourth panel demonstrates that DF-GMVI converges efficiently across all cases. However, it is important to note that when the posterior is Gaussian (Case A), DF-GMVI does not achieve exponential convergence due to the interactions among different Gaussian components; in contrast, Gaussian variational inference (2.10)[13] achieves exponential convergence in this setting. Furthermore, when the number of modes  $K$  is small, or when the initial Gaussian components are distant from the target mode, DF-GMVI may fail to capture all modes of the posterior density. Increasing  $K$  helps mitigate this issue and enhances performance.

We then modify these sampling problems to a 100-dimensional problem ( $N_\theta = 100$ ) by introducing  $N_\theta - 2$  additional variables,  $\theta^c$ . The reference density is defined with

$$\Phi_R(\theta, \theta^c) = \frac{1}{2} \mathcal{F}(\theta)^T \mathcal{F}(\theta) + \frac{1}{2} (\theta^c - K\theta)^T (\theta^c - K\theta),$$

where  $\theta \in \mathbb{R}^2$ ,  $\theta^c \in \mathbb{R}^{N_\theta - 2}$ , and  $K \in \mathbb{R}^{(N_\theta - 2) \times 2}$  is an all-ones matrix. The function  $\mathcal{F}$  is defined as in the previous 2-dimensional densities. These high-dimensional densities are constructed so that the marginal densities of  $\theta$  remain computable and identical to that of the previous 2-dimensional densities, which serves as the error indicator for evaluating DF-GDVI.

Similarly, we apply DF-GMVI with  $K = 10, 20$ , and  $40$  modes, each randomly initialized as  $\mathcal{N}(0, I)$  with equal weights. The marginal densities obtained from the estimated 100-dimensional densities at the 200th iteration are shown in Figure 3, using the same configuration as in Figure 2. The estimated marginal densities closely

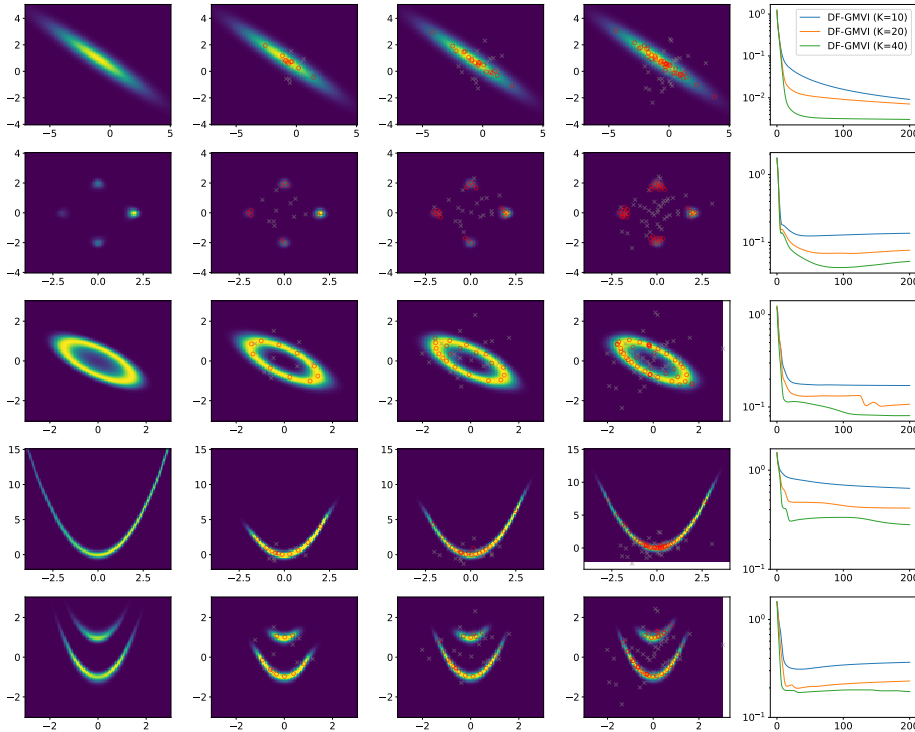


Fig. 2: Multi-dimensional problems with dimensionality 2, arranged from Case A to Case E from the top row to the bottom row. Each panel shows the reference density alongside the densities estimated by DF-GMVI with  $K = 10, 20$  and  $40$  (from left to right). The mean  $m_k$  of each Gaussian component is marked by red circles, and the initial means are marked by gray crosses. The fourth panel shows the total variation distance between the reference density and the densities estimated by the DF-GMVI over the iterations.

align with the reference, and the total variation distances are similar to those from the 2-dimensional problems in Figure 2. This confirms that the performance of DF-GMVI remains robust across different dimensionalities. We conjecture that the difficulty of the sampling problem depends primarily on the complexity of the target density (e.g., the number of modes) rather than the dimensionality.

Finally, we compare DF-GMVI with other state-of-the-art methods, including the Gaussian mixture approximation of the natural gradient flow (NGF-VI) (2.17) [41], its diagonal covariance variant (NGF-VI-D) [49], the Wasserstein gradient flow (WGF-VI) [40], BBVI [52], and the affine invariant MCMC method [27, 21]. NGF-VI, NGF-VI-D, and WGF-VI are not derivative free, requiring the computation of the gradient or Hessian of  $\Phi_R$ . Expectations are approximated using the mean-point approximation discussed in Appendix A. Motivated by the covariance positivity insight outlined in section 4, for the NGF-VI and NGF-VI-D, we implement an adaptive time-stepping scheme defined as

$$\Delta t = \min\left\{\Delta t_{\max}, \frac{\beta}{\max_k \|C_k \mathbb{E}_{\mathcal{N}_k} [\nabla_{\theta} \nabla_{\theta} \log \rho_a^{\text{GM}}(t) + \nabla_{\theta} \nabla_{\theta} \Phi_R]\|_2}\right\}$$

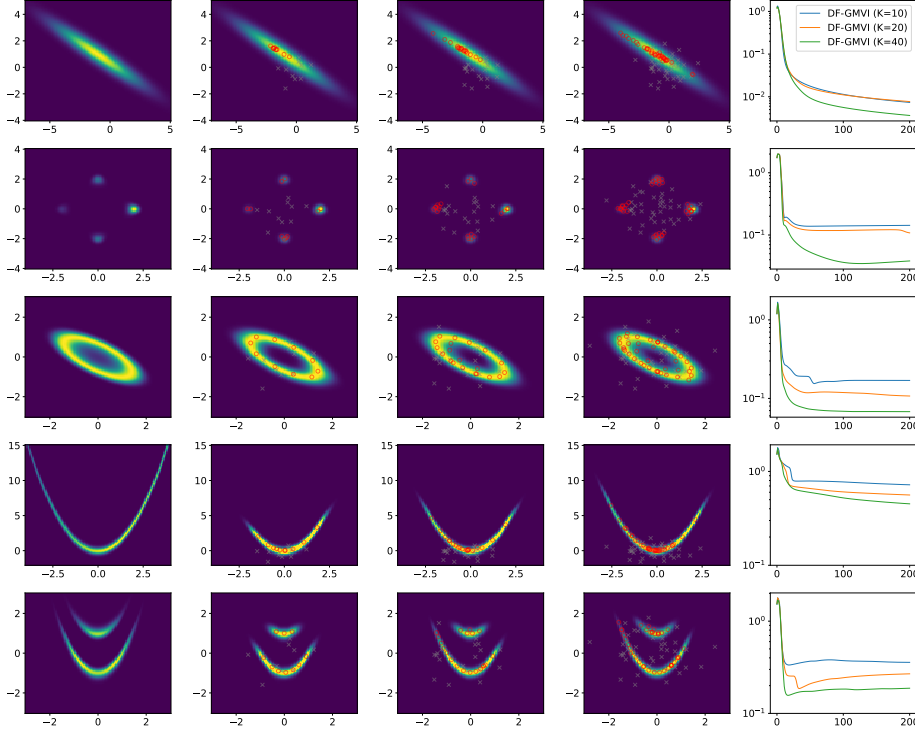


Fig. 3: Multi-dimensional problems with dimensionality 100, arranged from Case A to Case E from the top row to the bottom row. Each panel shows the marginal density of the reference alongside the marginal densities estimated by DF-GMVI with  $K = 10, 20$ , and  $40$  (from left to right). The projected means of each Gaussian component are marked by red circles, and the projected initial means are marked by grey crosses. The fourth panel displays the total variation between the reference marginal density and the estimated marginal densities across the iterations.

with  $\Delta t_{\max} = 0.5$  and  $\beta = 0.99$ , ensuring that the covariance update  $C_k^{-1}(t + \Delta t) = C_k^{-1}(t) + \Delta t \mathbb{E}_{\mathcal{N}_k}[\nabla_{\theta} \nabla_{\theta} \log \rho_a^{\text{GM}}(t) + \nabla_{\theta} \nabla_{\theta} \Phi_R]$  maintains positive definiteness. For the WGF-VI, the covariance update equation can be written as

$$\dot{C}_k^{-1} = C_k^{-1} \mathbb{E}_{\mathcal{N}_k} + \mathbb{E}_{\mathcal{N}_k} C_k^{-1}, \quad \mathbb{E}_{\mathcal{N}_k} = \mathbb{E}_{\mathcal{N}_k}[\nabla_{\theta} \nabla_{\theta} \log \rho_a^{\text{GM}}(t) + \nabla_{\theta} \nabla_{\theta} \Phi_R].$$

We follow the update method proposed in [40],  $C_k^{-1}(t + \Delta t) = M(t)C_k^{-1}(t)M(t)$ ,  $M(t) = I + \Delta t \mathbb{E}_k(t)$ , where  $I$  is the identity matrix, to achieve first-order accuracy while ensuring covariance positivity. The time step  $\Delta t$  is manually chosen to ensure stability, with values  $1.4 \times 10^{-1}$ ,  $5.0 \times 10^{-3}$ ,  $5.0 \times 10^{-3}$ ,  $4.0 \times 10^{-3}$  and  $8.0 \times 10^{-4}$  for Case A to Case E, respectively. For the BBVI, we adopt the natural gradient flow (2.17), derive the mean and covariance update equations by using integration by parts, as follows:

$$(5.1) \quad \begin{aligned} \dot{m}_k &= -\mathbb{E}_{\mathcal{N}_k}[(\theta - m_k)(\log \rho_a^{\text{GM}} + \Phi_R)], \\ \dot{C}_k &= -\mathbb{E}_{\mathcal{N}_k}[\left((\theta - m_k)(\theta - m_k)^T - C_k\right)(\log \rho_a^{\text{GM}} + \Phi_R)]. \end{aligned}$$



We apply the Monte Carlo method with 5 ensembles (same as DF-GMVI) to compute these integrals. We use empirical covariance instead of  $C_k$  in the right-hand-side of the covariance update equation to reduce variance, and implement a similar adaptive time-stepping scheme defined as

$$\Delta t = \min\left\{\Delta t_{\max}, \frac{\beta}{\max_k \|\mathbb{E}_{\mathcal{N}_k} [((\theta - m_k)(\theta - m_k)^T - C_k)(\log \rho_a^{\text{GM}} + \Phi_R)] C_k^{-1}\|_2}\right\}$$

with  $\Delta t_{\max} = 0.5$  and  $\beta = 0.99$ . Finally, for the affine invariant MCMC method, we use the stretch move method proposed in [27]. To recover the equilibrium distributions, we apply Gaussian kernel density estimation with a selectively chosen bandwidth using particles sampled from the last 10 iterations.

Figure 4 shows the results obtained using Gaussian mixture variational inference approaches with  $K = 40$  and the affine invariant MCMC method with  $J = 10^3$  particles for the 2-dimensional problems. We observe that these variational inference approaches require very small time steps, particularly in Case E, to ensure stability. Our proposed adaptive time steppers significantly improve this. The BBVI method exhibits random noise, which can be mitigated by increasing the ensemble size for Monte Carlo integrals. Among the variational inference methods, those based on natural gradient flows with affine invariance outperform their counterparts based on Wasserstein gradient flows. Overall, the results obtained by DF-GMVI, as shown in Figure 2, are similarly comparable and avoid the use of derivatives. In high dimensional spaces, the volume grows exponentially, which makes it difficult for random derivative free methods to explore the space efficiently. As a result, the performance of BBVI and derivative free MCMC methods typically deteriorates with increasing dimensionality, as illustrated in Figure 5. However, the quadrature rule Definition 3.1 leverages gradient structure, allowing our DF-GMVI method to avoid this issue even in the 100-dimensional problem. Consequently, our DF-GMVI method outperforms the other approaches on the test problems presented in this subsection.

**5.3. High-Dimensional Inverse Problem.** In this subsection, we study the problem of recovering the initial vorticity field,  $\omega_0$ , of a fluid flow based on measurements taken at later times. The flow is governed by the 2D incompressible Navier-Stokes equation on a periodic domain  $D = [0, 2\pi] \times [0, 2\pi]$ , written in the vorticity-streamfunction  $\omega - \psi$  formulation:

$$(5.2) \quad \begin{aligned} \frac{\partial \omega}{\partial t} + (v \cdot \nabla)\omega - \nu \Delta \omega &= \nabla \times f, \\ \omega &= -\Delta \psi \quad \frac{1}{4\pi^2} \int \psi = 0 \quad v = \left[\frac{\partial \psi}{\partial x_2}, -\frac{\partial \psi}{\partial x_1}\right]^T + v_b. \end{aligned}$$

Here  $v$  denotes the velocity vector,  $\nu = 0.01$  denotes the viscosity,  $v_b = [0, 2\pi]^T$  denotes the non-zero mean background velocity, and  $f(x) = [0, \cos(4x_{(1)})]^T$  denotes the external forcing.

The problem setup follows [14], which is spatially symmetric with respect to  $x_{(1)} = \pi$ . The source of the fluid is chosen such that  $\nabla \times f([x_{(1)}, x_{(2)}]^T) = -\nabla \times f([2\pi - x_{(1)}, x_{(2)}]^T)$ . The observations in the inverse problem are chosen as the difference of pointwise measurements of the vorticity value  $\omega([x_{(1)}, x_{(2)}]^T) - \omega([2\pi - x_{(1)}, x_{(2)}]^T)$  at 56 equidistant points in the left domain (see Figure 6), at  $T = 0.25$  and  $T = 0.5$ , corrupted with observation error  $\eta \sim \mathcal{N}(0, 0.1^2 I)$ . Under this set-up, both  $\omega_0([x_{(1)}, x_{(2)}]^T)$  and  $-\omega_0([2\pi - x_{(1)}, x_{(2)}]^T)$  will lead to the same measurements. Thus the posterior of the Bayesian inverse problem will be at least bi-modal.

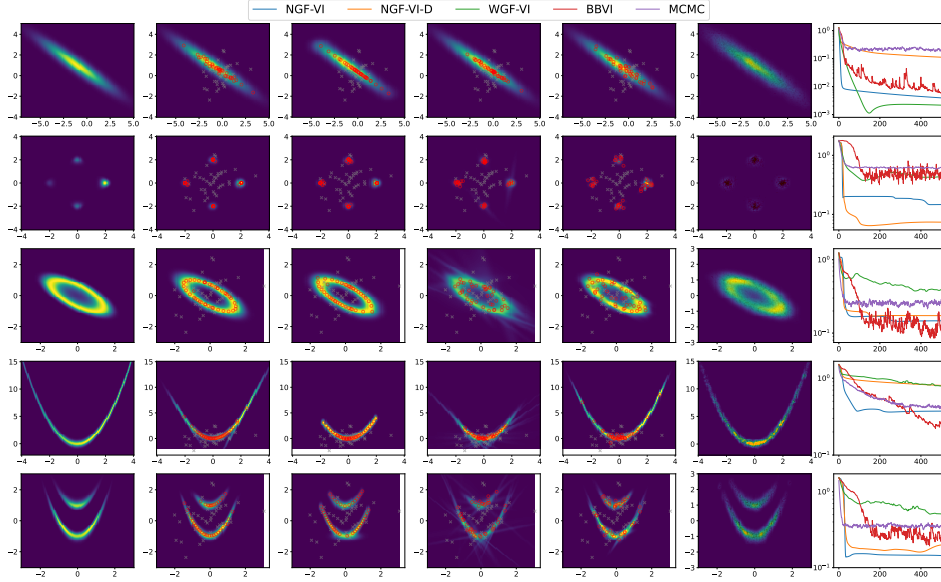


Fig. 4: Comparison study for multi-dimensional problems with dimensionality 2, arranged from Case A to Case E (from top to bottom). Each panel displays the reference density alongside the densities estimated by variational inference methods and the affine invariant MCMC (left to right: NGF-VI, NGF-VI-D, WGF-VI, BBVI, MCMC). The last figure shows the total variation distance between the reference density and the densities estimated by different methods over the iterations.

We assume the prior of  $\omega_0(x, \theta)$  is a Gaussian field with covariance operator  $C = (-\Delta)^{-2}$ , subject to periodic boundary conditions, on the space of mean zero functions. Following [28], let  $\mathbb{Z}_+^2 = \{(l_1, l_2) \in \mathbb{Z}^2, l_2 > 0\} \cup \{(l_1, 0) \in \mathbb{Z}^2, l_1 > 0\}$  and  $\mathbb{Z}_-^2 = -\mathbb{Z}_+^2$ , the corresponding KL expansion of the initial vorticity field is given by

$$(5.3) \quad \omega_0(x, \theta) = \sum_{l \in \mathbb{Z}^2 \setminus \{(0,0)\}} \theta_{(l)} \sqrt{\lambda_l} \psi_l(x),$$

where eigenpairs are of the form

$$\psi_l(x) = \begin{cases} \frac{\sin(l \cdot x)}{\sqrt{2\pi}} & l \in \mathbb{Z}_+^2 \\ \frac{\cos(l \cdot x)}{\sqrt{2\pi}} & l \in \mathbb{Z}_-^2 \end{cases} \quad \lambda_l = \frac{1}{|l|^4},$$

and  $\theta_{(l)} \sim \mathcal{N}(0, 2\pi^2)$ . The KL expansion (5.3) can be rewritten as a sum over positive integers, where the eigenvalues  $\lambda_l$  are in descending order. We truncate the expansion to the first 128 terms and generate the truth vorticity field  $\omega_0(x; \theta_{\text{ref}})$  with  $\theta_{\text{ref}} \in \mathbb{R}^{128}$ ; we aim to recover the parameters based on observation data.

We apply DF-GMVI with  $K = 3$  modes, initialized randomly according to the prior distribution and assigned equal weights. In Figure 7, we display the true initial vorticity field,  $\omega_0(x; \theta_{\text{ref}})$ , along with its mirrored field (where the mirroring of the velocity field induces antisymmetry in the vorticity field), and the three recovered initial vorticity fields,  $\omega_0(x; m_k)$ , obtained by DF-GMVI at the 200th iteration. Modes

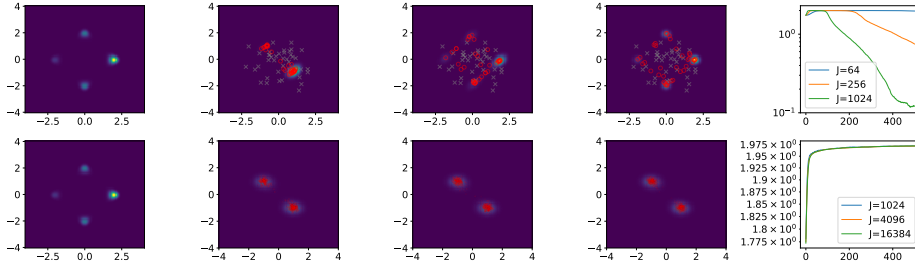


Fig. 5: Comparison study for multi-dimensional problems with dimensionality 100 (Case B). The figures display the marginal reference density and the estimated marginal densities obtained by BBVI with  $K = 40$  and ensemble sizes  $J = 64, 256,$  and  $1024$  for Monte Carlo integration, and by affine invariant MCMC method with ensemble sizes  $J = 2^{10}, 2^{12},$  and  $2^{14}$  (from left to right). The last figure shows the total variation distance between the marginal reference density and the estimated marginal densities over iterations.

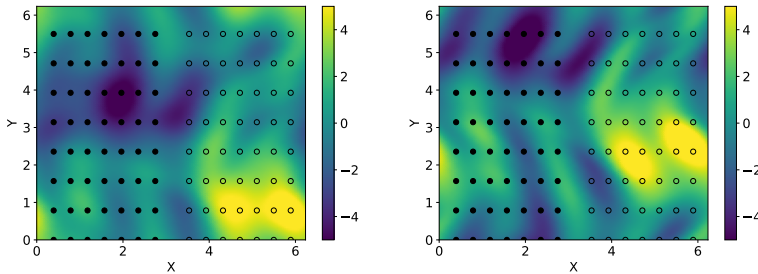


Fig. 6: The vorticity field  $\omega$  at  $T = 0.25$  and  $T = 0.5$  and observations  $\omega([x_{(1)}, x_{(2)}]^T) - \omega([2\pi - x_{(1)}, x_{(2)}]^T)$  at 56 equidistant points (solid black dots). Their mirroring points are marked (empty black dots).

1 and 2 capture  $\omega_0(x; \theta_{\text{ref}})$ , while mode 3 captures the mirrored field of  $\omega_0(x; \theta_{\text{ref}})$  itself. Figure 8 illustrates the relative errors in the vorticity field, optimization errors  $\Phi_R(m_k)$ , the Frobenius norm  $\|C_k\|_F$ , and the Gaussian mixture weights  $w_k$  (left to right) at each iteration. This demonstrates that DF-GMVI converges in fewer than 50 iterations. Figure 9 shows the marginal distributions of the estimated posterior for the first 16  $\theta_{(l)}$ -coefficients obtained by DF-GMVI. The marginal distributions reveal clear bimodality, with the approximate posterior placing high probability mass around the true coefficients while also capturing the alternative possibility (the mirrored value). This example demonstrates DF-GMVI's potential for effectively handling multimodal posteriors in large-scale, high-dimensional applications.

**6. Conclusion.** In this paper, we have explored guidelines, such as covariance positivity and affine invariance, to design stable derivative free Gaussian variational methods. Based on these guidelines, we have introduced DF-GMVI as an effective approach for solving Bayesian inverse problems. Our numerical experiments demonstrate the superior stability of DF-GMVI and its capability to approximate complex

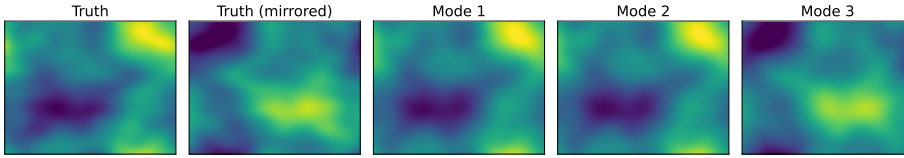


Fig. 7: The true initial vorticity field  $\omega_0(x; \theta_{\text{ref}})$ , and recovered initial vorticity fields  $\omega_0(x; m_k)$  obtained by DF-GMVI.

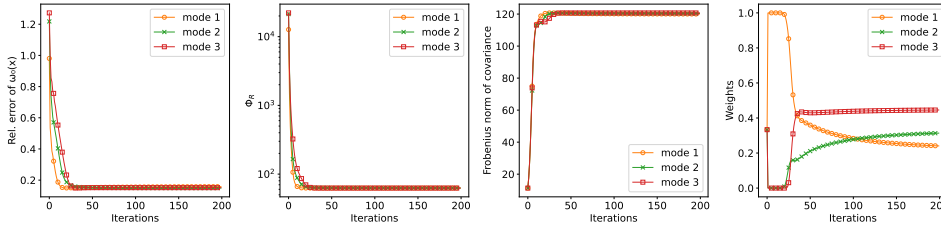


Fig. 8: Navier-Stokes flow problem: the relative errors of the initial vorticity field, the optimization errors  $\Phi_R(m_k)$ , the Frobenius norm  $\|C_k\|_F$ , and the Gaussian mixture weights  $w_k$  (from left to right) for different modes over iterations.

high dimensional posterior distributions. There are several promising directions for future research. On the algorithmic side, developing stable derivative free variational inference methods beyond Bayesian inverse problems (1.2) would be valuable. On the theoretical side, a thorough analysis of the stability and convergence properties of the natural gradient flow (2.17) with Gaussian mixtures and DF-GMVI for general posterior densities, including log-concave densities, could provide important insights for their practical applications.

**Acknowledgments.** DZH acknowledges the high-performance computing platform at Peking University. YC acknowledges support from the Courant Instructorship.

**Appendix A. Quadrature Rule Comparison.** In this section, we compare various quadrature rules, including mean-point approximation, unscented [38, 36] and cubature [2] transformations, for approximating Gaussian integrations in solving the natural gradient flow (2.17). We examine a 2-dimensional Gaussian mixture target density, with  $\Phi_R(\theta) = -\log\left(\sum_{i=1}^3 w_i \mathcal{N}(\theta; m_i, C_i)\right)$ , where  $w_1 = 0.2$ ,  $m_1 = \begin{bmatrix} 1 \\ 2 \end{bmatrix}$ ,  $C_1 = I$ ,  $w_2 = 0.5$ ,  $m_2 = \begin{bmatrix} 2 \\ 1 \end{bmatrix}$ ,  $C_2 = I$ , and  $w_3 = 0.3$ ,  $m_3 = \begin{bmatrix} -1 \\ -1 \end{bmatrix}$ ,  $C_3 = I/2$ . We implement gradient and Hessian of  $\Phi_R(\theta)$ , and consider four combinations for the quadrature integrations, (1) both  $\Phi_R$  and  $\log \rho_a$  related terms integrated with mean-point approximation, (2) both  $\Phi_R$  and  $\log \rho_a$  related terms integrated with unscented transformation using weight  $\sqrt{3}$  [38, 36], (3) both  $\Phi_R$  and  $\log \rho_a$  related terms integrated with the third-order cubature transformation [2], and (4)  $\Phi_R$  related terms integrated with mean-point approximation and  $\log \rho_a$  related terms with third-order cubature transformation. We use  $K = 10$ ,  $\Delta t = 0.02$ , and solving for 1000 iterations,

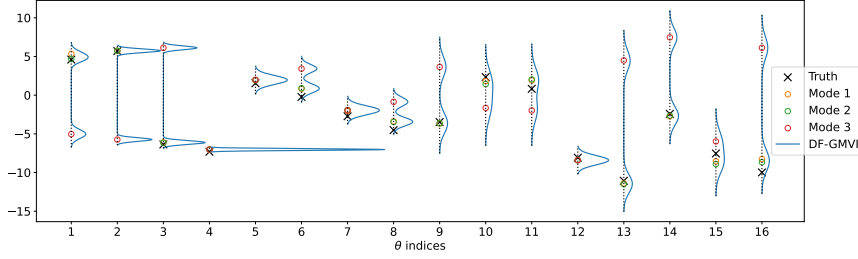


Fig. 9: Navier-Stokes flow problem: the true Karhunen-Loeve expansion parameters  $\theta_{(i)}$  (black crosses), and mean estimations of  $\theta_{(i)}$  for each modes (circles) and the associated marginal distributions obtained by DF-GMVI at the 50th iteration.

the convergence results are presented in Figure 10. In the context of solving gradient flow, the mean-point approximation achieves superior convergence, even though it is not the most accurate quadrature rule. And hence the mean-point approximation is used in Definitions 3.1 and 3.2.

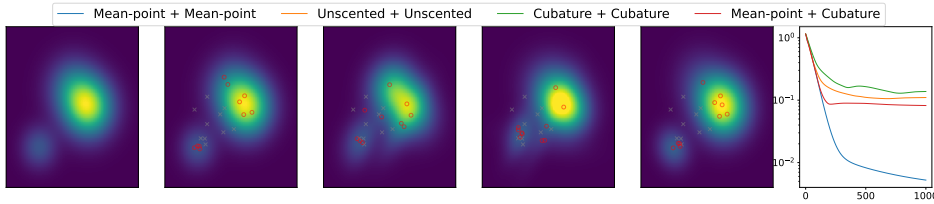


Fig. 10: Quadrature rule comparison for the Gaussian mixture target density problem. Each panel displays the reference density and densities estimated by approximating natural gradient flow (2.17) with various quadrature rule combinations (from left to right). The mean  $m_k$  (red circles) and initial mean (grey crosses) of each Gaussian component are marked. The last panel shows the total variation distance between the reference density and the densities estimated.

## Appendix B. Proof of Proposition 4.2.

*Proof.* We note that

$$\nabla_{\theta} \Phi_R(\theta) = T^T \nabla_{\tilde{\theta}} \tilde{\Phi}_R(\tilde{\theta}), \quad \nabla_{\theta} \nabla_{\theta} \Phi_R(\theta) = T^T \nabla_{\tilde{\theta}} \nabla_{\tilde{\theta}} \tilde{\Phi}_R(\tilde{\theta}) T.$$

1. To prove the affine invariance of the natural gradient flow defined by (2.17), it suffices to verify that under the affine mapping

$$\tilde{w}_k = w_k, \quad \tilde{m}_k = T m_k + d, \quad \tilde{C}_k = T C_k T^T,$$

$\tilde{w}_k, \tilde{m}_k$  and  $\tilde{C}_k$  also satisfy the corresponding equation (2.17). We simplify the notation by  $\tilde{\mathcal{N}}_k(\tilde{\theta}) = \mathcal{N}(\tilde{\theta}, \tilde{m}_k, \tilde{C}_k)$ ,  $\rho_{\tilde{a}}^{\text{GM}}(\tilde{\theta}) = \sum_{k=1}^K \tilde{w}_k \tilde{\mathcal{N}}_k(\tilde{\theta})$ . We have  $\tilde{\mathcal{N}}_k(\tilde{\theta}) = |\det T|^{-1} \mathcal{N}_k(\theta)$ ,  $\rho_{\tilde{a}}^{\text{GM}}(\tilde{\theta}) = |\det T|^{-1} \rho_a^{\text{GM}}(\theta)$ , and thus  $\nabla_{\tilde{\theta}} \log \rho_{\tilde{a}}^{\text{GM}}(\tilde{\theta}) =$   $\blacksquare$

$T^{-T}\nabla_\theta \log \rho_a^{\text{GM}}(\theta)$ ,  $\nabla_{\tilde{\theta}}\nabla_{\tilde{\theta}}\log \rho_a^{\text{GM}}(\tilde{\theta}) = T^{-T}\nabla_\theta \nabla_\theta \log \rho_a^{\text{GM}}(\theta)T^{-1}$ . By these equations and change-of-variable formula, we have that

$$\begin{aligned}
\dot{\tilde{m}}_k &= T\dot{m}_k = -TC_k \int \mathcal{N}_k(\theta) \left( \nabla_\theta \log \rho_a^{\text{GM}}(\theta) + \nabla_\theta \Phi_R(\theta) \right) d\theta \\
&= -TC_k T^T \int \tilde{\mathcal{N}}_k(\tilde{\theta}) T^{-T} \left( \nabla_\theta \log \rho_a^{\text{GM}}(\theta) + \nabla_\theta \Phi_R(\theta) \right) d\tilde{\theta} \\
&= -\tilde{C}_k \int \tilde{\mathcal{N}}_k(\tilde{\theta}) \left( \nabla_{\tilde{\theta}} \log \rho_a^{\text{GM}}(\tilde{\theta}) + \nabla_{\tilde{\theta}} \tilde{\Phi}_R(\tilde{\theta}) \right) d\tilde{\theta}, \\
\dot{\tilde{C}}_k &= T\dot{C}_k T^T = -TC_k \left( \int \mathcal{N}_k(\theta) (\nabla_\theta \nabla_\theta \log \rho_a^{\text{GM}}(\theta) + \nabla_\theta \nabla_\theta \Phi_R(\theta)) d\theta \right) C_k T^T \\
&= -TC_k T^T \left( \int \tilde{\mathcal{N}}_k(\tilde{\theta}) T^{-T} (\nabla_\theta \nabla_\theta \log \rho_a^{\text{GM}}(\theta) + \nabla_\theta \nabla_\theta \Phi_R(\theta)) T^{-1} d\tilde{\theta} \right) TC_k T^T \\
&= -\tilde{C}_k \left( \int \tilde{\mathcal{N}}_k(\tilde{\theta}) (\nabla_{\tilde{\theta}} \nabla_{\tilde{\theta}} \log \rho_a^{\text{GM}}(\tilde{\theta}) + \nabla_{\tilde{\theta}} \nabla_{\tilde{\theta}} \tilde{\Phi}_R(\tilde{\theta})) d\tilde{\theta} \right) \tilde{C}_k, \\
\dot{\tilde{w}}_k &= \dot{w}_k = -w_k \int \left( \mathcal{N}_k(\theta) - \rho_a^{\text{GM}}(\theta) \right) (\log \rho_a^{\text{GM}}(\theta) + \Phi_R(\theta)) d\theta \\
&= -\tilde{w}_k \int \left( \tilde{\mathcal{N}}_k(\tilde{\theta}) - \rho_a^{\text{GM}}(\tilde{\theta}) \right) (\log |\det T| + \log \rho_a^{\text{GM}}(\tilde{\theta}) + \tilde{\Phi}_R(\tilde{\theta})) d\tilde{\theta} \\
&= -\tilde{w}_k \int \left( \tilde{\mathcal{N}}_k(\tilde{\theta}) - \rho_a^{\text{GM}}(\tilde{\theta}) \right) (\log \rho_a^{\text{GM}}(\tilde{\theta}) + \tilde{\Phi}_R(\tilde{\theta})) d\tilde{\theta},
\end{aligned}$$

where in the last equality, we used the fact that  $\tilde{\mathcal{N}}_k$  and  $\rho_a^{\text{GM}}$  are both densities and thus  $\int (\tilde{\mathcal{N}}_k(\tilde{\theta}) - \rho_a^{\text{GM}}(\tilde{\theta})) \log |\det T| d\tilde{\theta} = 0$ . This completes the proof.

2. To prove that the DF-GMVI algorithm (3.8) is  $\mathcal{T}$ -invariant, it suffices to show that the quadrature rules defined in Definition 3.1 and Definition 3.2 satisfy the following equations for any  $T \in \mathcal{T}$ :

(B.1)

$$\begin{aligned}
\text{QR}_{\tilde{\mathcal{N}}_k} \{ \nabla_{\tilde{\theta}} \nabla_{\tilde{\theta}} \log \rho_a^{\text{GM}} + \nabla_{\tilde{\theta}} \nabla_{\tilde{\theta}} \tilde{\Phi}_R \} &= T^{-T} \text{QR}_{\mathcal{N}_k} \{ \nabla_\theta \nabla_\theta \log \rho_a^{\text{GM}} + \nabla_\theta \nabla_\theta \Phi_R \} T^{-1}, \\
\text{QR}_{\tilde{\mathcal{N}}_k} \{ \nabla_{\tilde{\theta}} \log \rho_a^{\text{GM}} + \nabla_{\tilde{\theta}} \tilde{\Phi}_R \} &= T^{-T} \text{QR}_{\mathcal{N}_k} \{ \nabla_\theta \log \rho_a^{\text{GM}} + \nabla_\theta \Phi_R \}, \\
\text{QR}_{\tilde{\mathcal{N}}_k} \{ \log \rho_a^{\text{GM}} + \tilde{\Phi}_R \} &= \text{QR}_{\mathcal{N}_k} \{ \log \rho_a^{\text{GM}} + \Phi_R \} - \log |\det T|.
\end{aligned}$$

Here in the last equality, we can tolerate a constant difference since we will normalize  $w_k(t + \Delta t)_{k=1}^K$  after the update (3.8). Given any Gaussian density  $\mathcal{N} = \mathcal{N}(\theta; m, C)$ , an affine mapping transforms it to another Gaussian  $\tilde{\mathcal{N}} = \mathcal{N}(\tilde{\theta}; \tilde{m}, \tilde{C})$ . The square root matrix computed by Cholesky decomposition satisfies  $\sqrt{\tilde{C}} = \sqrt{TC T^T} = T\sqrt{C}$ , when  $T$  is an invertible lower triangular matrix. Hence, the quadrature points generated for the two Gaussian densities according to Definition 3.1 satisfy

$$\begin{aligned}
\tilde{\theta}_0 &= \tilde{m} = Tm + d = T\theta_0 + d, \\
\tilde{\theta}_i &= \tilde{m} + \alpha[\sqrt{\tilde{C}}]_i = Tm + d + \alpha T[\sqrt{C}]_i = T\theta_i + d, \\
\tilde{\theta}_{N_\theta+i} &= \tilde{m} - \alpha[\sqrt{\tilde{C}}]_i = Tm + d - \alpha T[\sqrt{C}]_i = T\theta_{N_\theta+i} + d,
\end{aligned}$$

for  $1 \leq i \leq N_\theta$ . These equations imply that  $\tilde{\mathcal{F}}(\tilde{\theta}_i) = \mathcal{F}(\theta_i)$  for  $0 \leq i \leq 2N_\theta$ , and thus  $\tilde{c} = c$ ,  $\tilde{b}_i = b_i$ ,  $\tilde{a}_i = a_i$  for  $1 \leq i \leq N_\theta$ , and then  $\tilde{B} = B$ ,  $\tilde{A} = A$ .

Consequently,

(B.2)

$$\begin{aligned} \text{QR}_{\tilde{\mathcal{N}}}\{\tilde{\Phi}_R\} &= \frac{1}{2}\tilde{c}^T\tilde{c} = \frac{1}{2}c^Tc = \text{QR}_{\mathcal{N}}\{\Phi_R\}, \\ \text{QR}_{\tilde{\mathcal{N}}}\{\nabla_{\tilde{\theta}}\tilde{\Phi}_R\} &= \sqrt{\tilde{C}}^{-T}\tilde{B}^T\tilde{c} = T^{-T}\sqrt{C}^{-T}B^TC = T^{-T}\text{QR}_{\mathcal{N}}\{\nabla_{\theta}\Phi_R\}, \\ \text{QR}_{\tilde{\mathcal{N}}}\{\nabla_{\tilde{\theta}}\nabla_{\tilde{\theta}}\tilde{\Phi}_R\} &= \sqrt{\tilde{C}}^{-T}(6\text{Diag}(\tilde{A}^T\tilde{A}) + \tilde{B}^T\tilde{B})\sqrt{\tilde{C}}^{-1} \\ &= T^{-T}\sqrt{C}^{-T}(6\text{Diag}(A^TA) + B^TB)\sqrt{C}^{-1}T^{-1} \\ &= T^{-T}\text{QR}_{\mathcal{N}}\{\nabla_{\theta}\nabla_{\theta}\Phi_R\}T^{-1}. \end{aligned}$$

By the [Definition 3.2](#), we have that

(B.3)

$$\begin{aligned} \text{QR}_{\tilde{\mathcal{N}}_k}\{\log \rho_a^{\text{GM}}\} &= \log \rho_a^{\text{GM}}(\tilde{m}_k) = \log(|\det T|^{-1}\rho_a^{\text{GM}}(m_k)) = \text{QR}_{\mathcal{N}_k}\{\log \rho_a^{\text{GM}}\} - \log|\det T|, \\ \text{QR}_{\tilde{\mathcal{N}}_k}\{\nabla_{\tilde{\theta}}\log \rho_a^{\text{GM}}\} &= \nabla_{\tilde{\theta}}\log \rho_a^{\text{GM}}(\tilde{m}_k) = T^{-T}\nabla_{\theta}\log \rho_a^{\text{GM}}(m_k) = T^{-T}\text{QR}_{\mathcal{N}_k}\{\nabla_{\theta}\log \rho_a^{\text{GM}}\}. \end{aligned}$$

Using the same notations as in [Definition 3.2](#), we have  $\tilde{v}_i(\tilde{\theta}) = \tilde{C}_i^{-1}(\tilde{\theta} - \tilde{m}_i) = (TC_iT^T)^{-1}(T\theta - Tm_i) = T^{-T}v_i(\theta)$ , and thus it is easy to check that

$$(B.4) \quad \text{QR}_{\tilde{\mathcal{N}}_k}\{\nabla_{\tilde{\theta}}\nabla_{\tilde{\theta}}\log \rho_a^{\text{GM}}\} = T^{-T}\text{QR}_{\mathcal{N}_k}\{\nabla_{\theta}\nabla_{\theta}\log \rho_a^{\text{GM}}\}T^{-1}.$$

Combining (B.2), (B.3) and (B.4), we finish the proof of (B.1).  $\square$

#### REFERENCES

- [1] S.-I. AMARI, *Natural gradient works efficiently in learning*, Neural computation, 10 (1998), pp. 251–276.
- [2] I. ARASARATNAM AND S. HAYKIN, *Cubature kalman filters*, IEEE Transactions on automatic control, 54 (2009), pp. 1254–1269.
- [3] M. J. BERGER, P. COLELLA, ET AL., *Local adaptive mesh refinement for shock hydrodynamics*, Journal of computational Physics, 82 (1989), pp. 64–84.
- [4] A. BESKOS, A. JASRA, E. A. MUZAFFER, AND A. M. STUART, *Sequential monte carlo methods for bayesian elliptic inverse problems*, Statistics and Computing, 25 (2015), pp. 727–737.
- [5] D. M. BLEI, A. KUCUKELBIR, AND J. D. MCAULIFFE, *Variational inference: A review for statisticians*, Journal of the American statistical Association, 112 (2017), pp. 859–877.
- [6] R. BORKER, D. HUANG, S. GRIMBERG, C. FARHAT, P. AVERY, AND J. RABINOVITCH, *Mesh adaptation framework for embedded boundary methods for computational fluid dynamics and fluid-structure interaction*, International Journal for Numerical Methods in Fluids, 90 (2019), pp. 389–424.
- [7] C. J. T. BRAAK, *A markov chain monte carlo version of the genetic algorithm differential evolution: easy bayesian computing for real parameter spaces*, Statistics and Computing, 16 (2006), pp. 239–249.
- [8] M. BURGER, M. ERBAR, F. HOFFMANN, D. MATTHES, AND A. SCHLICHTING, *Covariance-modulated optimal transport and gradient flows*, arXiv preprint arXiv:2302.07773, (2023).
- [9] S. CAO AND D. Z. HUANG, *Bayesian calibration for large-scale fluid structure interaction problems under embedded/immersed boundary framework*, International Journal for Numerical Methods in Engineering, (2022).
- [10] J. CARRILLO AND U. VAES, *Wasserstein stability estimates for covariance-preconditioned fokker-planck equations*, Nonlinearity, 34 (2021), p. 2275.
- [11] J. A. CARRILLO, Y. CHEN, D. Z. HUANG, J. HUANG, AND D. WEI, *Fisher-rao gradient flow: geodesic convexity and functional inequalities*, arXiv preprint arXiv:2407.15693, (2024).
- [12] J. A. CARRILLO, K. CRAIG, AND F. S. PATACCHINI, *A blob method for diffusion*, Calculus of Variations and Partial Differential Equations, 58 (2019), pp. 1–53.
- [13] Y. CHEN, D. Z. HUANG, J. HUANG, S. REICH, AND A. M. STUART, *Sampling via gradient flows in the space of probability measures*, arXiv preprint arXiv:2310.03597, (2023).

- [14] Y. CHEN, D. Z. HUANG, J. HUANG, S. REICH, AND A. M. STUART, *Efficient, multimodal, and derivative-free bayesian inference with fisher-rao gradient flows*, *Inverse Problems*, 40 (2024), p. 125001.
- [15] G. DETOMMASO, T. CUI, Y. MARZOUK, A. SPANTINI, AND R. SCHEICHL, *A stein variational newton method*, *Advances in Neural Information Processing Systems*, 31 (2018).
- [16] M. Z. DIAO, K. BALASUBRAMANIAN, S. CHEWI, AND A. SALIM, *Forward-backward gaussian variational inference via jko in the bures-wasserstein space*, in *International Conference on Machine Learning*, PMLR, 2023, pp. 7960–7991.
- [17] C. DOMINGO-ENRICH AND A.-A. POOLADIAN, *An explicit expansion of the kullback-leibler divergence along its fisher-rao gradient flow*, *Trans. Mach. Learn. Res.*, 2023 (2023), <https://api.semanticscholar.org/CorpusID:257102914>.
- [18] A. DOUCET, A. M. JOHANSEN, ET AL., *A tutorial on particle filtering and smoothing: Fifteen years later*, *Handbook of nonlinear filtering*, 12 (2009), p. 3.
- [19] J. ELFRING, E. TORTA, AND R. VAN DE MOLENGRAFT, *Particle filters: A hands-on tutorial*, *Sensors*, 21 (2021), p. 438.
- [20] G. EVENSEN, *Sequential data assimilation with a nonlinear quasi-geostrophic model using monte carlo methods to forecast error statistics*, *Journal of Geophysical Research: Oceans*, 99 (1994), pp. 10143–10162.
- [21] D. FOREMAN-MACKEY, D. W. HOGG, D. LANG, AND J. GOODMAN, *emcee: the mcmc hammer*, *Publications of the Astronomical Society of the Pacific*, 125 (2013), p. 306.
- [22] A. GARBUNO-INGO, F. HOFFMANN, W. LI, AND A. M. STUART, *Interacting langevin diffusions: Gradient structure and ensemble kalman sampler*, *SIAM Journal on Applied Dynamical Systems*, 19 (2020), pp. 412–441.
- [23] V. GAYRARD, A. BOVIER, M. ECKHOFF, AND M. KLEIN, *Metastability in reversible diffusion processes i: Sharp asymptotics for capacities and exit times*, *Journal of the European Mathematical Society*, 6 (2004), pp. 399–424.
- [24] V. GAYRARD, A. BOVIER, AND M. KLEIN, *Metastability in reversible diffusion processes ii: Precise asymptotics for small eigenvalues*, *Journal of the European Mathematical Society*, 7 (2005), pp. 69–99.
- [25] A. GELMAN, W. R. GILKS, AND G. O. ROBERTS, *Weak convergence and optimal scaling of random walk metropolis algorithms*, *The annals of applied probability*, 7 (1997), pp. 110–120.
- [26] C. J. GEYER, *Practical markov chain monte carlo*, *Statistical science*, (1992), pp. 473–483.
- [27] J. GOODMAN AND J. WEARE, *Ensemble samplers with affine invariance*, *Communications in applied mathematics and computational science*, 5 (2010), pp. 65–80.
- [28] M. HAIRER AND J. C. MATTINGLY, *Ergodicity of the 2d navier-stokes equations with degenerate stochastic forcing*, *Annals of Mathematics*, (2006), pp. 993–1032.
- [29] M. D. HOFFMAN, D. M. BLEI, C. WANG, AND J. PAISLEY, *Stochastic variational inference*, *Journal of Machine Learning Research*, (2013).
- [30] D. Z. HUANG, P. AVERY, C. FARHAT, J. RABINOVITCH, A. DERKEVORKIAN, AND L. D. PETERSON, *Modeling, simulation and validation of supersonic parachute inflation dynamics during mars landing*, in *AIAA Scitech 2020 Forum*, 2020, p. 0313.
- [31] D. Z. HUANG, D. DE SANTIS, AND C. FARHAT, *A family of position-and orientation-independent embedded boundary methods for viscous flow and fluid-structure interaction problems*, *Journal of Computational Physics*, 365 (2018), pp. 74–104.
- [32] D. Z. HUANG, J. HUANG, S. REICH, AND A. M. STUART, *Efficient derivative-free bayesian inference for large-scale inverse problems*, *Inverse Problems*, 38 (2022), p. 125006.
- [33] D. Z. HUANG, T. SCHNEIDER, AND A. M. STUART, *Iterated kalman methodology for inverse problems*, *Journal of Computational Physics*, 463 (2022), p. 111262.
- [34] T. HUIX, A. KORBA, A. DURMUS, AND E. MOULINES, *Theoretical guarantees for variational inference with fixed-variance mixture of gaussians*, *arXiv preprint arXiv:2406.04012*, (2024).
- [35] R. JORDAN, D. KINDERLEHRER, AND F. OTTO, *The variational formulation of the fokker-planck equation*, *SIAM journal on mathematical analysis*, 29 (1998), pp. 1–17.
- [36] S. JULIER, J. UHLMANN, AND H. DURRANT-WHYTE, *A new method for the nonlinear transformation of means and covariances in filters and estimators*, *IEEE Transactions on Automatic Control*, 45 (2000), pp. 477–482, <https://doi.org/10.1109/9.847726>.
- [37] S. J. JULIER AND J. K. UHLMANN, *New extension of the kalman filter to nonlinear systems*, in *Signal processing, sensor fusion, and target recognition VI*, vol. 3068, *International Society for Optics and Photonics*, 1997, pp. 182–193.
- [38] S. J. JULIER, J. K. UHLMANN, AND H. F. DURRANT-WHYTE, *A new approach for filtering nonlinear systems*, in *Proceedings of 1995 American Control Conference-ACC'95*, vol. 3, *IEEE*, 1995, pp. 1628–1632.



- [39] J. KAIPIO AND E. SOMERSALO, *Statistical and computational inverse problems*, vol. 160, Springer Science & Business Media, 2006.
- [40] M. LAMBERT, S. CHEWI, F. BACH, S. BONNABEL, AND P. RIGOLLET, *Variational inference via wasserstein gradient flows*, Advances in Neural Information Processing Systems, 35 (2022), pp. 14434–14447.
- [41] W. LIN, M. E. KHAN, AND M. SCHMIDT, *Fast and simple natural-gradient variational inference with mixture of exponential-family approximations*, in International Conference on Machine Learning, PMLR, 2019, pp. 3992–4002.
- [42] Q. LIU, *Stein variational gradient descent as gradient flow*, Advances in neural information processing systems, 30 (2017).
- [43] T. LIU, P. GHOSAL, K. BALASUBRAMANIAN, AND N. PILLAI, *Towards understanding the dynamics of gaussian-stein variational gradient descent*, Advances in Neural Information Processing Systems, 36 (2024).
- [44] I. LOPEZ-GOMEZ, C. D. CHRISTOPOULOS, H. L. ERVIK, O. R. DUNBAR, Y. COHEN, AND T. SCHNEIDER, *Training physics-based machine-learning parameterizations with gradient-free ensemble kalman methods*, (2022).
- [45] Y. LU, D. SLEPČEV, AND L. WANG, *Birth–death dynamics for sampling: global convergence, approximations and their asymptotics*, Nonlinearity, 36 (2023), p. 5731, <https://doi.org/10.1088/1361-6544/acf988>, <https://dx.doi.org/10.1088/1361-6544/acf988>.
- [46] J. MARTENS, *New insights and perspectives on the natural gradient method*, Journal of Machine Learning Research, 21 (2020), pp. 1–76, <http://jmlr.org/papers/v21/17-678.html>.
- [47] A. MAURAS AND Y. MARZOUK, *Sampling in unit time with kernel fisher-rao flow*, arXiv preprint arXiv:2401.03892, (2024).
- [48] N. MOËS, J. DOLBOW, AND T. BELYTSCHKO, *A finite element method for crack growth without remeshing*, International journal for numerical methods in engineering, 46 (1999), pp. 131–150.
- [49] D. H. NGUYEN, T. SAKURAI, AND H. MAMITSUKA, *Wasserstein gradient flow over variational parameter space for variational inference*, arXiv preprint arXiv:2310.16705, (2023).
- [50] M. OPPER AND C. ARCHAMBEAU, *The variational gaussian approximation revisited*, Neural computation, 21 (2009), pp. 786–792.
- [51] C. S. PESKIN, *Numerical analysis of blood flow in the heart*, Journal of computational physics, 25 (1977), pp. 220–252.
- [52] R. RANGANATH, S. GERRISH, AND D. BLEI, *Black box variational inference*, in Artificial intelligence and statistics, PMLR, 2014, pp. 814–822.
- [53] C. R. RAO, *Information and the accuracy attainable in the estimation of statistical parameters*, Reson. J. Sci. Educ, 20 (1945), pp. 78–90.
- [54] T. SCHNEIDER, S. LAN, A. STUART, AND J. TEIXEIRA, *Earth system modeling 2.0: A blueprint for models that learn from observations and targeted high-resolution simulations*, Geophysical Research Letters, 44 (2017), pp. 12–396.
- [55] M. K. SEN AND P. L. STOFFA, *Global optimization methods in geophysical inversion*, Cambridge University Press, 2013.
- [56] A. SMITH, *Sequential Monte Carlo methods in practice*, Springer Science & Business Media, 2013.
- [57] A. M. STUART, *Inverse problems: a bayesian perspective*, Acta numerica, 19 (2010), pp. 451–559.
- [58] Z. TAN, C. M. KAUL, K. G. PRESSEL, Y. COHEN, T. SCHNEIDER, AND J. TEIXEIRA, *An extended eddy-diffusivity mass-flux scheme for unified representation of subgrid-scale turbulence and convection*, Journal of Advances in Modeling Earth Systems, 10 (2018), pp. 770–800.
- [59] C. TEBALDI, R. L. SMITH, D. NYCHKA, AND L. O. MEARNES, *Quantifying uncertainty in projections of regional climate change: A Bayesian approach to the analysis of multimodel ensembles*, Journal of Climate, 18 (2005), pp. 1524–1540.
- [60] J. A. VRUGT, C. J. TER BRAAK, C. G. DIKS, B. A. ROBINSON, J. M. HYMAN, AND D. HIGDON, *Accelerating markov chain monte carlo simulation by differential evolution with self-adaptive randomized subspace sampling*, International journal of nonlinear sciences and numerical simulation, 10 (2009), pp. 273–290.
- [61] M. J. WAINWRIGHT, M. I. JORDAN, ET AL., *Graphical models, exponential families, and variational inference*, Foundations and Trends® in Machine Learning, 1 (2008), pp. 1–305.
- [62] M. WELANDAWE, M. R. ANDERSEN, A. VEHTARI, AND J. H. HUGGINS, *A framework for improving the reliability of black-box variational inference*, Journal of Machine Learning Research, 25 (2024), pp. 1–71.
- [63] J.-J. ZHU AND A. MIELKE, *Kernel approximation of fisher-rao gradient flows*, arXiv preprint arXiv:2410.20622, (2024).